



# Petrophysical rock typing based on the diagenetic effect of the different microfacies types of Abu Madi clastic reservoir in Faraskur Gas Field, onshore Nile Delta, Egypt

Emad A. Eysa<sup>1</sup> · Bassem S. Nabawy<sup>2</sup> · Ashraf Ghoneimi<sup>1</sup> · Ahmed H. Saleh<sup>1</sup>

Received: 6 September 2023 / Accepted: 11 November 2023 / Published online: 20 December 2023  
© The Author(s) 2023

## Abstract

The sandstone of Abu Madi clastic reservoir constitutes the prime gas-producing reservoir in the Nile Delta region. So, the present research aims to delineate its microfacies and dominant diagenetic features and their effect on the petrophysical characteristics of the Abu Madi reservoir in the Faraskur Gas Field. This could be achieved by integrating the petrographical studies and the conventional data to divide the reservoir into some reservoir rock types (RRTs) to delineate the impact of the mineral composition and diagenetic features on their reservoir quality and hydraulic flow zones. Petrographically, most samples are immature and described as angular to subrounded, poorly sorted, and slightly cemented. Five clastic microfacies types are recorded in the Abu Madi Formation: (1) quartz arenite, (2) feldspathic quartz arenite, (3) sub-feldspathic quartz arenite, (4) quartz wacke, and (5) sub-feldspathic quartz wacke. The most important post-depositional processes affecting the reservoir quality are the precipitation of pyrite and microsparite, as well as the feldspars alteration into authigenic dispersed clays represented by kaolinite and smectite/illite mixed layers. The dominant pore types are the primary intergranular, with some subsidiary fractures and dissolution pores. To check the reservoir quality of the Abu Madi clastics, the NPI (normalized porosity index), FZI (flow zone indicator), RQI (reservoir quality index), and  $\lambda_k$  (permeability anisotropy) were estimated. Petrophysically, the studied samples are summed up into four RRTs, with the RRT4 group has the lowest  $\varnothing$  and  $k$  values (av.  $\varnothing = 16.2\%$ , av.  $k_H = 6.87$  mD) and the lowest reservoir quality parameters (av. FZI = 0.89  $\mu\text{m}$ , av. DRT = 10.4, av. RQI = 0.18  $\mu\text{m}$ , av.  $R_{35} = 1.26$   $\mu\text{m}$ ). On the contrary, the RRT1 group has the best petrophysical and reservoir parameters (av.  $\varnothing = 25.9\%$ , av.  $k_H = 2695$  mD, av. DRT = 14.9, av. RQI = 3.12  $\mu\text{m}$ , av. FZI = 8.85  $\mu\text{m}$ , av.  $R_{35} = 32.7$   $\mu\text{m}$ ). The permeability anisotropy of the RRT2 and RRT3 is the highest in Faraskur Field (av.  $\lambda_k = 2.4$  and 2.62, respectively). This study is applicable to other extensions of the Abu Madi reservoirs in the Nile Delta basin to help in predicting their reservoir quality, petrophysical properties, and their hydrocarbon potentiality.

**Keywords** Faraskur · Nile Delta · Abu Madi · Diagenesis · Petrophysics · Reservoir quality

## List of symbols

|                 |                               |
|-----------------|-------------------------------|
| $\varnothing_e$ | Effective porosity (%)        |
| $k$             | Air permeability (mD)         |
| $k_H$           | Horizontal permeability (mD)  |
| $k_V$           | Vertical permeability (mD)    |
| $\lambda_k$     | Permeability anisotropy (0.0) |
| $\rho_b$        | Bulk density (g/cc)           |
| $\rho_g$        | Grain density (g/cc)          |

|          |  |
|----------|--|
| $R_{35}$ | Effective pore radius estimated at 35% mercury injection capillary pressure technique (MICP) |
| $R^2$    | Correlation coefficient  |

## Abbreviations

|       |  |
|-------|--|
| DRT   | Discrete rock type                           |
| EGPC  | Egyptian General Petroleum Corporation       |
| FZI   | Flow zone indicator                          |
| LST   | Low-stand tract                              |
| NPI   | Normalized porosity index                    |
| ROUND | Is an excel function for rounding the values |
| RQI   | Reservoir quality index                      |
| RRT   | Reservoir rock type                          |
| TST   | Transgressive-system tract                   |
| XRD   | X-ray diffraction                            |

✉ Emad A. Eysa  
emad\_eysa@zu.edu.eg

<sup>1</sup> Geology Department, Faculty of Science, Zagazig University, Zagazig, Egypt

<sup>2</sup> Department of Geophysical Sciences, National Research Center, Cairo, Egypt

## Introduction

During the last decades, the northern Nile Delta province has had the main development and exploration plans in Egypt. It produced several TCF (trillions of cubic feet) of natural gas during the last decades from various gas-bearing clastic reservoirs of Oligocene to Pliocene–Pleistocene age (Pigott and Abdel-Fattah 2014; Abdel-Fattah 2014; Nabawy et al. 2018; Sarhan and Safa 2019; Sarhan 2021a, b; Fawzy et al. 2022). Recently, the gas reserve of these fields has been increased due to applying some enhanced recovery techniques, e.g., chemical enhanced recovery as recommended by many authors (e.g., Bigdeli and Delshad 2023). Since the Nile Delta is fluvial in origin, it consists primarily of thick shale sequences intercalated with some sand beds, lobes, and lenses that resulted from the seasonal activities of the Nile valley in the Pliocene–Quaternary time (Nabawy and Shehata 2015). These clastic sequences are capped by a thick silty clay layer of Holocene age that increases in thickness to the north (Abd-Allah et al. 2012; Nabawy and Shehata 2015). Due to the progressive exploration/development activities in the Nile Delta, its daily gas production increased from 4 BCF/day in 2015 to about 7.1 BCF/day in 2018. Most of the Nile Delta's gas-producing fields produce hydrocarbons from the Late Miocene Messinian Abu Madi Formation which has been the main gas-producing horizon since its discovery in 1966 when the first well in the Nile Delta (Mit Ghamr-1 well) was drilled (Abu El-Ella 1990; Sarhan 2022). It is stated that Abu Madi clastics are the main gas reservoir and the main target for many exploration consortiums in both onshore and offshore Nile Delta.

Abu Madi Formation produces gas from many gas fields in the onshore/offshore Nile Delta, e.g., Abu Madi, Baltim, Faraskur, South Batra, Abu Qir, Nidoco, El-Qar'a, etc. (Nabawy and Shehata 2015; Ghoneimi et al. 2017; Sarhan and Safa 2019; Sarhan 2021a, b; Safa et al. 2021; Leila et al. 2021; Othman et al. 2022; Nabawy et al. 2023). Among these, the Faraskur Gas Field, the target of this study, is in the northern onshore Nile Delta at longitudes 31°13'48" and 31°24'36" E and latitudes 31°21'36" and 31°37'12" N (Fig. 1).

A few literatures investigated the Faraskur Gas Field (e.g., Leila et al. 2021); they paid more attention to the structural setting interpretation using seismic data and the petrophysical analysis using the well log data. Therefore, the present work aims to continue and improve these studies with more attention to the microfacies analysis and diagenetic features impact on the reservoir quality and petrophysical characters derived from the core data. It is targeted to evaluate the Abu Madi gas-bearing clastics in Faraskur Field based on the routine core data (Rcal) and

the petrographic studies to delineate the implementation of various microfacies and the predominant diagenetic features on the different reservoir properties. Core data and petrographical studies were integrated to assess the reservoir parameters of the Abu Madi reservoir qualitatively and quantitatively.

Integrating the core data and petrographical studies to delineate the reservoir quality, the main hydraulic flow zones, and the main diagenetic features controlling the reservoir properties is a well-known procedure that is applied by many researchers (e.g., El Sawy et al. 2020; Nabawy et al. 2020a, b, c; Leila et al. 2021, 2022; Elhossainy et al. 2021; Sarhan 2021a, b; Nabawy et al. 2022a, b; Radwan et al. 2022a, b; Fallah-Bagtash et al. 2022; Ashoor et al. 2023; Elmahdy et al. 2023).

Thereby, the reservoir quality and flow zones discrimination were also applied using the permeability and porosity data, where the reservoir quality index (RQI) can be used to evaluate the reservoir flow character and to establish a set of interrelationships among the various petrophysical parameters at the core plug and the well bore scales. The petrographical data include thin sections and X-ray diffraction data, which are used to delineate the microfacies types, mineralogical compositions, and diagenetic features that affected the Abu Madi reservoir.

## Geologic setting

The Nile Delta Basin is a fan-shaped area of 250,000 km<sup>2</sup>; it is among the main deltaic basins in the world (Sestini 1989; Kirschbaum et al. 2010). It is located along the southern shoreline of the Mediterranean Basin and situated on the northern borders of the colliding African plate. It is located among three tectonic plates: the Syrian Arc fold system, the Red Sea Rift, and the African-Anatolian plates (Harms and Wary 1990; Sarhan and Hemdan 1994).

Geologically, the Nile Delta is built of the Nile submarine fan, the continental slope, and the continental shelf (from North Sinai to 80 km west of Alexandria). It is situated at the northern margins of the African plate and constitutes a part of the southern Mediterranean shorelines. Its structural setting is primarily controlled by the breakup of the African plate margin accompanied by the northward movement of the Arabian plate and the Red Sea opening (Said 1981). The main diagnostic structural feature of the Nile Delta is its central Hinge Zone that controls the sedimentary facies distribution in the Nile Delta (Fig. 2) (Abdel Aal et al. 1994; Sarhan and Hemdan 1994; Kamel et al. 1998; Nabawy and Shehata 2015; Nabawy et al. 2018). The Hinge Zone subdivides the Nile Delta into two structural provinces (northern basin and southern block) (Fig. 2).

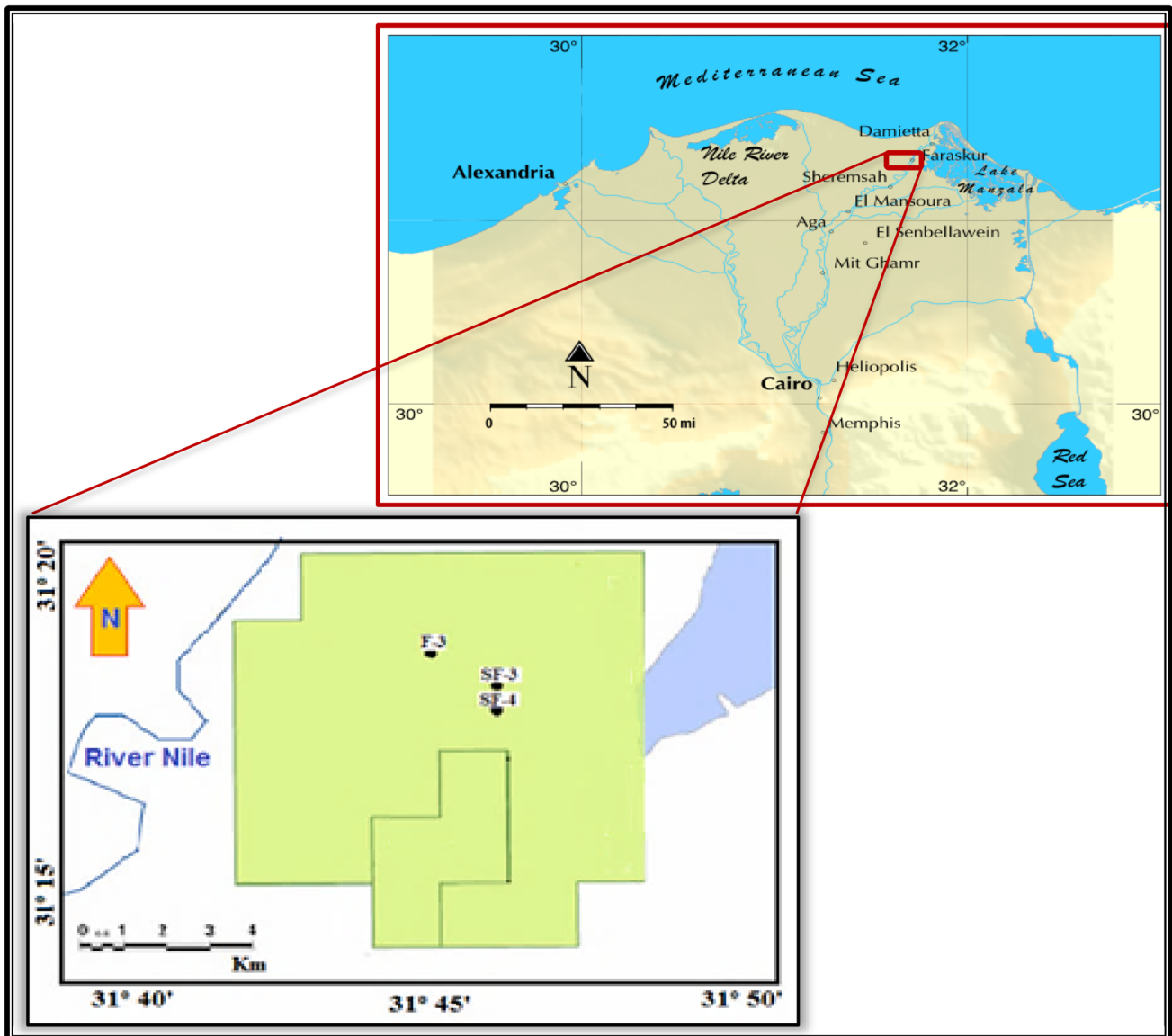


Fig. 1 Location map of the studied Faraskur Gas Field, onshore north Nile Delta, Egypt

The Nile Delta northern basin is configured by a set of regional tectonic elements oriented in different trends. Some of these structural features were active during the Miocene to cause tilting of the Miocene depositional sequence.

The Nile Delta is dominated by thrust faulting, diagnostic asymmetric folds, and diapers. These are caused by the implication of Syrian Arc movements trending NE-SW along the northern Nile Delta basin. Due to its importance, the subsurface and structural geology of the Nile Delta northern basin has been explored by eminent authors (e.g., Rizzini et al. 1978; Barakat 1982; Schlumberger 1984; EGPC 1994; Mosconi et al. 1996; Abu El Ata et al. 1999; Mahsoub 2006; Khaled et al. 2014; Elhamy and Salah 2016; etc.). The natural gas of this northern basin has been

generated and accumulated at various stratigraphic zones varying from the Oligocene upward to Pliocene rock units.

The stratigraphic sequence of the Nile Delta province extends from the Jurassic to the Pleistocene (Fig. 3).

The Miocene sediments of the Nile Delta northern basin have been paid attention by many researchers due to their huge subsurface gas-bearing reservoirs (Niazi and Dahi 2004; Vandre et al. 2007; Leila et al. 2016 and Abd El-Gawad et al. 2019). In particular, the explored natural gas in the Messinian Abu Madi Formation has been a prime target for researchers since 1967 in its onshore occurrences and offshore extensions (Abu El-Ella 1990). The Miocene depositional cycle starts with open marine sediments and ends with a starved evaporitic sequence. It can be subdivided

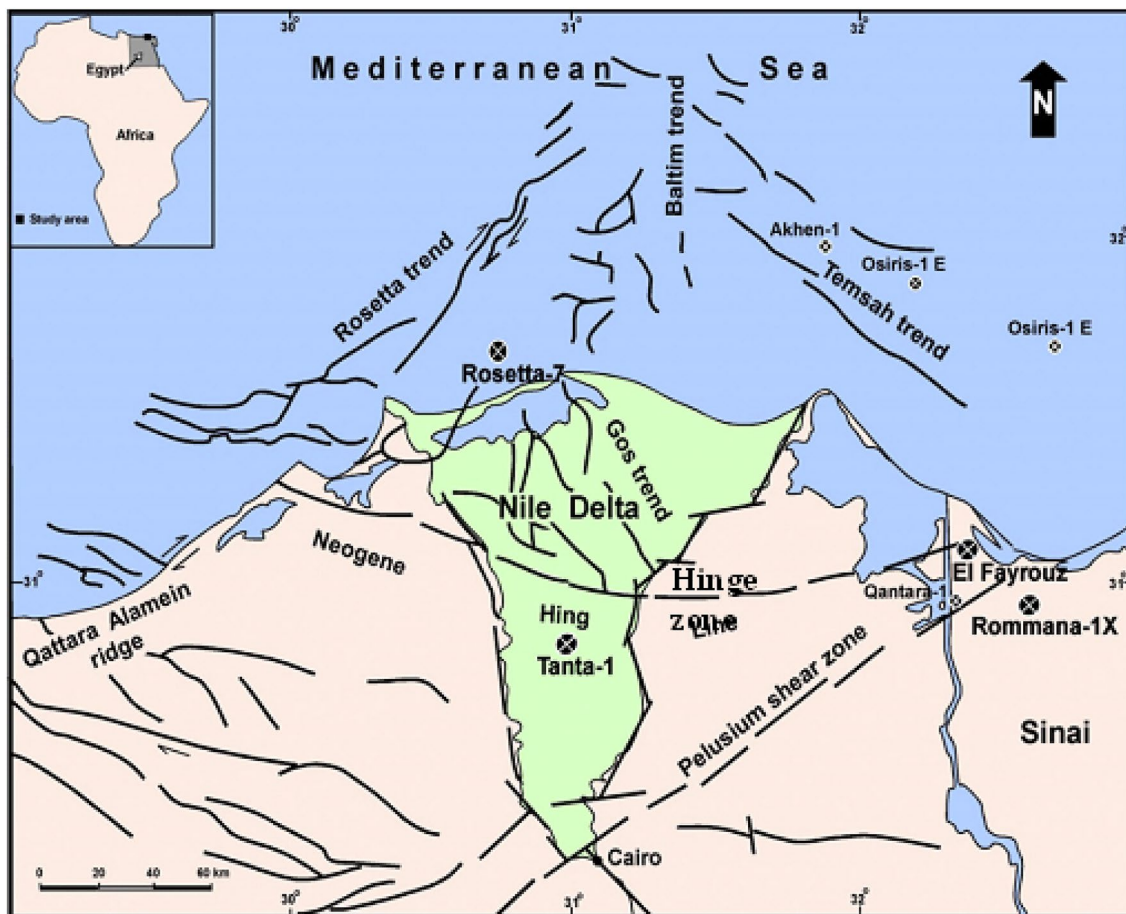


Fig. 2 Location map showing the main structural trends of the Nile Delta (Abdel Aal et al. 1994)

into the Oligo-Miocene Qantara Formation, Middle Miocene Sidi Salim Formation, and the Upper Miocene Qawasim and Abu Madi Formations and their equivalent Rosetta evaporites (Fig. 3; EGPC 1994; Sultan et al. 2020). However, the Abu Madi Formation is the most important gas-bearing horizon in the Nile Delta basin; it constitutes the best clastic reservoir in the Nile Delta with very good porosity values averaging 21% (EGPC 1994).

Tectonically, the Messinian Abu Madi reservoir represents the topmost sequence of the Upper Miocene that is controlled by the evolution of the syn-rift mega sequence of the Nile Delta (Sarhan 2022). It rests uncomfortably, in the northern Nile Delta basin, on the Qawasim Formation and/or the Rosetta evaporites (El-Heiny 1982; El-Heiny and Morsi 1992; EGPC 1994; Barakat and Dominik 2010; Barakat 2010) (Fig. 3). It consists of thick sandstone beds, rarely conglomerate, intercalated exhibiting shale beds with more thickness and abundance along the topmost parts of the Abu Madi reservoir. The sand grains are primarily loose quartzose and vary in size from very fine

to coarse-grained. The conglomeratic zones at the lower parts of the Abu Madi Formation represent an unconformity with the Qawasim Formation.

The Abu Madi reservoir has been accumulated as a channel fill presenting low-stand fluvial system tracts (LST) and transgressive-system tracts (TST) of estuarine sedimentary setting (Salem et al. 2005). The facies distribution of the Abu Madi Formation has been affected by the paleogeomorphology that was controlled by the rapid deposition on low-stand erosion surface and faulting at the Late Messinian (El Heiny et al. 1990).

It is stated that the Abu Madi reservoir is characterized by cross-bedded sandstone and shale content, which increases in dominance upwards (EGPC 1994; El Heiny and Enani 1996).

The Abu Madi reservoir mainly consists of a set of transgressive facies as it consists mainly of reworked lithic fragments from the Qawasim and Pre-Qawasim Formations (Rizzini et al. 1978; Barber 1981).



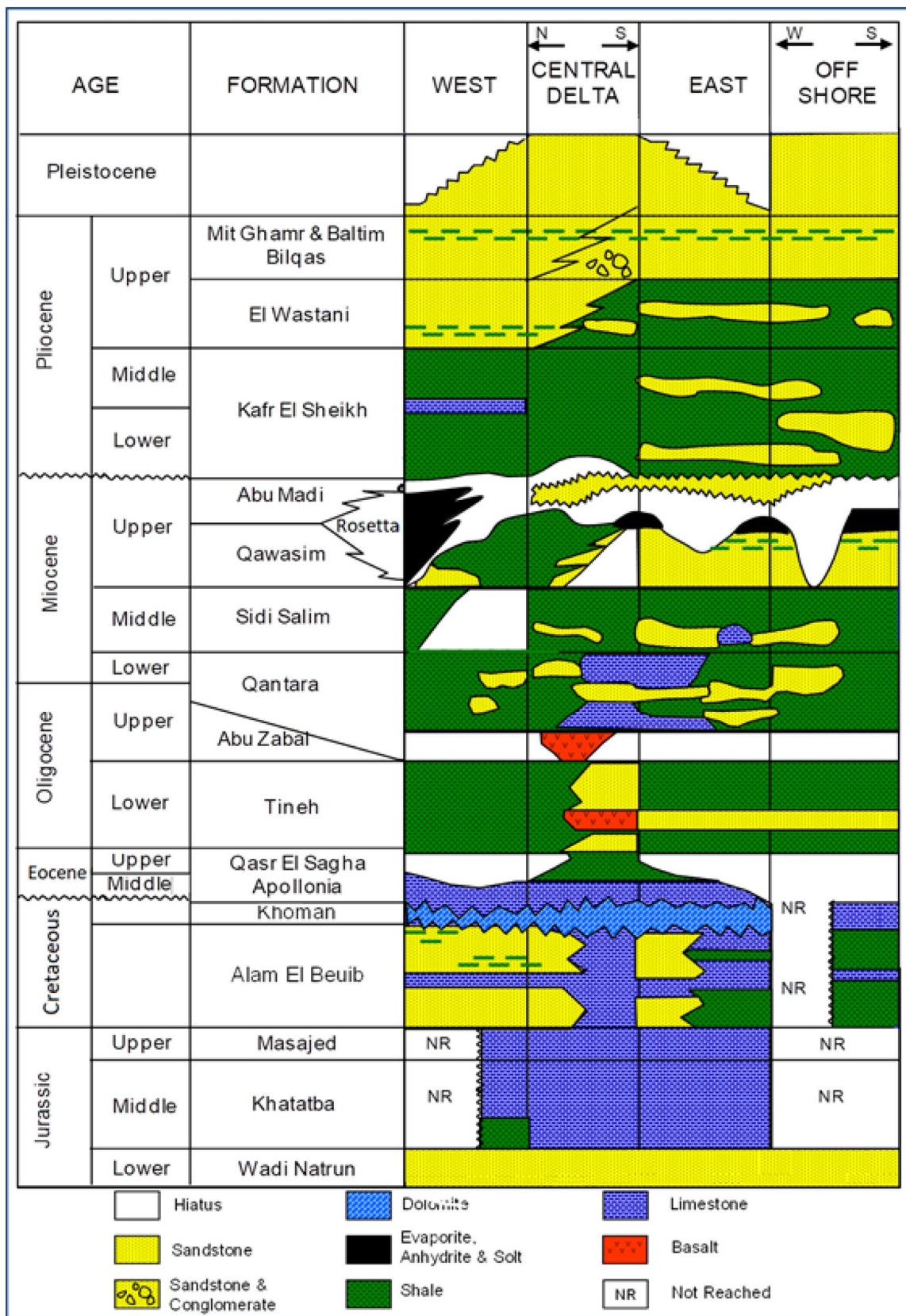


Fig. 3 Generalized lithostratigraphic sections of the Nile Delta (modified after EGPC 1994; Sultan et al. 2020)

## Methods and techniques

### Core data

Eighty-three plug samples are available for the core measurements (33 samples from S. Faraskur-3 well and 50 samples from S. Faraskur-4 well). Plugging has been applied representatively for the Abu Madi reservoir at core depth intervals 2625–2638 m for S. Faraskur-3 well and 2818–2838 m for S. Faraskur-4 well. The grain density ( $\rho_g$ ) and porosity ( $\varnothing_{He}$ ) were measured using a helium pycnometer at 19 psi, while the gas permeability ( $k$ ) was measured using a nitrogen permeameter. Measuring permeability has been applied for two plugs/depth points and oriented horizontally and vertically ( $k_H$  and  $k_V$ ). Details on the applied procedures are published in many literature (e.g., Nabawy and Wassif 2017; Nabawy and El Aal 2019a, b; Abuhagaza et al. 2021; Shehata et al. 2021; Radwan et al. 2021, 2022a; Radwan and Nabawy 2022). Anisotropy of the measured permeability was calculated using the following mathematical model as mentioned by many researchers (Serra 1988; Nabawy 2018; Abdeen et al. 2021; Nabawy et al. 2022a).

$$\lambda_k = \sqrt{\frac{k_H}{k_V}} \quad (1)$$

For ranking the quality of the Abu Madi sandstone reservoir, the NPI (normalized porosity index), FZI (flow zone indicator), and the RQI (reservoir quality index) parameters of Amaefule et al. (1993) were applied as recommended by several researchers (Corbett & Potter 2004; Teh et al. 2012; Abed 2014; Abuamarah and Nabawy 2021; Fallah-Bagtash et al. 2022). These parameters were calculated using the following equations.

$$NPI = \frac{\varnothing}{1 - \varnothing} \quad (2)$$

$$RQI = 0.0314 \sqrt{\frac{k}{\varnothing}} \quad (3)$$

$$FZI = \frac{RQI}{NPI} \quad (4)$$

where  $\varnothing$  is the porosity in fraction,  $k$  is the permeability in md, while NPI is estimated in fraction, and the RQI and FZI are estimated in  $\mu\text{m}$ .

For ranking the petrophysical and reservoir parameters of the Abu Madi reservoir, the classification ranks of Nabawy et al. (2015) and Nabawy and El Sharawy (2018) were applied. These ranks were successfully applied by many researchers (e.g., Nabawy et al. 2010, 2020b, c; Ashoor et al. 2023).

Rock typing was also used for grouping the available core data based on the porosity and permeability values supported by the DRT (discrete rock types) of Shenawi et al. (2007). It was improved later by Nabawy and El Sharawy (2018). The DRT parameter is estimated from the FZI, which in turn is based on porosity and permeability.

$$DRT = \text{ROUND}(2 \times \text{Ln}(FZI) + 10.6; 1) \quad (5)$$

where the FZI is expressed in  $\mu\text{m}$  and can be calculated using Eq. (4).

Also, the  $R_{35}$  of Winland (1972) was estimated using the following equation.

$$\text{Log } R_{35} = 0.732 + 0.588 \text{Log } k - 0.864 \text{Log } \varnothing \quad (6)$$

The statistical processing parameters of the available core data are listed in Table 1.

### Petrographical data

For studying the lithologic composition, sedimentary fabrics, and the predominated diagenetic features of Abu Madi samples, a total of 69 impregnated and stained thin sections were prepared representatively for the different rock types. These samples were impregnated by blue-dyed Araldite for studying the pore fabrics and declaring the different pore types. They are also stained with a mixture of potassium ferricyanide and Alizarin Red-S solutions to differentiate between the calcite, Mg-rich calcite, and dolomite. The alkali-feldspars can be also detected by staining the samples with a Na Cobaltinitrite ( $\text{Na}_3\text{Co}(\text{NO}_2)_6$ ) solution.

Grain size analysis was applied using sieve analysis for the selected 69 samples from the prospective sandstone horizons along the cored interval. Besides, an additional 10 samples were prepared as fine powders to analyze their dominant clay composition where the clay fraction has been isolated and analyzed using the X-ray diffraction (XRD) technique. The results of the mineral composition of the various microfacies are listed in Table 2.

## Results

### Core data

Petrophysically, the Abu Madi samples are grouped into 4 RRTs (Table 1). The RRT4 samples have the lowest permeability and porosity (av.  $\varnothing = 16.2\%$ , av.  $k_H = 6.87$  md; Table 1, respectively) and the lowest reservoir quality parameters (av.  $DRT = 10.4$ , av.  $R_{35} = 1.26 \mu\text{m}$ , av.  $FZI = 0.89 \mu\text{m}$ , av.  $RQI = 0.18 \mu\text{m}$ , Table 1, respectively). On the contrary, the RRT1 samples are characterized by the highest petrophysical parameters in the Faraskur

**Table 1** Petrophysical core data of the Abu Madi Formation in S. Faraskur-3 well, onshore Nile Delta, Egypt

| RRTs | S. no | Microfacies  |      | DRT<br>0.00 | $k_H$<br>mD | $k_V$<br>mD | $\lambda_k$<br>0.00 | $\varnothing_{He}$<br>% | $\rho_g$<br>g/cc | $\rho_b$<br>g/cc | RQI<br>$\mu\text{m}$ | FZI<br>$\mu\text{m}$ | $R_{35}$<br>$\mu\text{m}$ |
|------|-------|--|------|-------------|-------------|-------------|---------------------|-------------------------|------------------|------------------|----------------------|----------------------|---------------------------|
| RRT1 | 8     | Quartz arenite   | Min  | 14.6        | 1216        | 266.0       | 1.15                | 22.5                    | 2.639            | 1.892            | 2.31                 | 7.55                 | 23.9                      |
|      |       |  | Max  | 15.5        | 5149        | 1632        | 3.05                | 28.3                    | 2.691            | 2.086            | 4.31                 | 11.48                | 47.2                      |
|      |       |  | Mean | 14.9        | 2695        | 1099.5      | 1.68                | 25.9                    | 2.665            | 1.975            | 3.12                 | 8.85                 | 32.7                      |
| RRT2 | 26    | Quartz arenite<br>Feldspathic quartz arenite<br>Subfeldspathic quartz arenite                  | Min  | 13.1        | 322         | 0.95        | 0.85                | 23.3                    | 2.646            | 1.864            | 1.13                 | 3.41                 | 10.0                      |
|      |       |  | Max  | 14.4        | 2494        | 1343        | 18.4                | 30.6                    | 2.767            | 2.086            | 2.84                 | 6.78                 | 28.1                      |
|      |       |  | Mean | 13.8        | 972.5       | 460.6       | 2.4                 | 26.5                    | 2.678            | 1.968            | 1.80                 | 4.92                 | 17.1                      |
| RRT3 | 69    | Quartz arenite<br>Quartz wacke<br>Subfeldspathic quartz arenite<br>Subfeldspathic quartz wacke | Min  | 11.0        | 3.54        | 0.07        | 0.37                | 11.7                    | 2.636            | 1.848            | 0.17                 | 1.19                 | 1.35                      |
|      |       |  | Max  | 13.0        | 605.0       | 438.0       | 51.5                | 30.2                    | 2.702            | 2.352            | 1.41                 | 3.39                 | 12.4                      |
|      |       |  | Mean | 12.1        | 169.1       | 105.6       | 2.62                | 23.8                    | 2.668            | 2.032            | 0.73                 | 2.24                 | 6.11                      |
| RRT4 | 21    | Feldspathic quartz arenite<br>Quartz wacke<br>Subfeldspathic quartz wacke                      | Min  | 9.7         | 1.03        | 0.18        | 0.28                | 11.0                    | 2.611            | 2.009            | 0.09                 | 0.65                 | 0.68                      |
|      |       |  | Max  | 10.9        | 23.0        | 121.0       | 4.88                | 25.0                    | 2.762            | 2.417            | 0.31                 | 1.19                 | 2.25                      |
|      |       |  | Mean | 10.4        | 6.87        | 19.2        | 1.49                | 16.2                    | 2.667            | 2.235            | 0.18                 | 0.89                 | 1.26                      |

DRT is the discreet rock type (Shenawi et al. 2007; El Sharawy and Nabawy 2018; Nabawy and El Sharawy 2018),  $k_H$  and  $k_V$  are the permeability values in the horizontal and vertical directions, respectively;  $\lambda_k$  is the permeability anisotropy;  $\varnothing_{He}$  is the helium porosity;  $\rho_g$  and  $\rho_b$  are the grain and bulk densities; RQI is the reservoir quality index; FZI is the flow zone indicator; and  $R_{35}$  is the effective pore radius at 35% mercury saturation (Winland 1972)

**Table 2** XRD results of the clay fractions for some representative samples selected from S. Faraskur-3 and S. Faraskur-4 wells

| Well          | Sample no. | Microfacies type                      | Depth m | Smectite/illite mixed % | Illite % | Chlorite % | Kaolinite % |
|---------------|------------|---------------------------------------|---------|-------------------------|----------|------------|-------------|
| S. Faraskur-3 | 1          | RRT3<br>Subfeldspathic quartz arenite | 2818.2  | –                       | Traces   | –          | 100         |
|               | 2          | RRT3<br>Subfeldspathic quartz arenite | 2825.5  | 3                       | 4        | –          | 93          |
|               | 3          | RRT2<br>Feldspathic quartz arenite    | 2826.5  | 53                      | 18       | –          | 29          |
|               | 4          | RRT2<br>Subfeldspathic quartz wacke   | 2835.1  | 65                      | 4        | –          | 31          |
|               | 5          | RRT2<br>Subfeldspathic quartz wacke   | 2837.5  | 55                      | 5        | –          | 40          |
| S. Faraskur-4 | 6          | RRT4<br>Subfeldspathic quartz wacke   | 2628.0  | 60                      | –        | –          | 40          |
|               | 7          | RRT2<br>Quartz arenite                | 2630.0  | –                       | –        | –          | 100         |
|               | 8          | RRT3<br>Subfeldspathic quartz arenite | 2632.0  | –                       | –        | –          | 100         |
|               | 9          | RRT1<br>Quartz arenite                | 2634.0  | –                       | –        | –          | 100         |
|               | 10         | RRT2<br>Quartz arenite                | 2636.0  | –                       | –        | –          | 100         |

Field (av.  $\varnothing = 25.9\%$ , av.  $k_H = 2695$  md, av. DRT = 14.9, av. RQI = 3.12  $\mu\text{m}$ , av. FZI = 8.85  $\mu\text{m}$ , av.  $R_{35} = 32.7$   $\mu\text{m}$ , Table 1, respectively). The RRT2 and the RRT3 are considered transitional groups (av. DRT = 13.8 and 12.1,

respectively, Table 1) characterized by midway petrophysical properties and reservoir quality parameters between the RRT1 and the RRT4 samples. The permeability anisotropy



of these two RRTs is the highest in Faraskur Field (av.  $\lambda_k = 2.4$  and 2.62, respectively, Table 1).

### Lithofacies types

The identified lithofacies types of the Abu Madi can be grouped into two lithofacies associations: (1) Arenites and (2) Mudstones.

#### Arenite lithofacies

The lithofacies description of the studied reservoir sequence indicates that the dominated arenites are composed of seven lithofacies: (1) glauconitic bedded sandstone, (2) glauconitic massive sandstone, (3) laminated sandstone, (4) glauconitic sandstone, (5) deformed, laminated and glauconitic sandstone, (6) glauconitic argillaceous sandstone, and (7) glauconitic, pebbly sandstone. These lithofacies types are characterized by gray to greenish gray color due to their high glauconite content. They are also characterized by some diagnostic sedimentary structures, e.g., massive and blocky

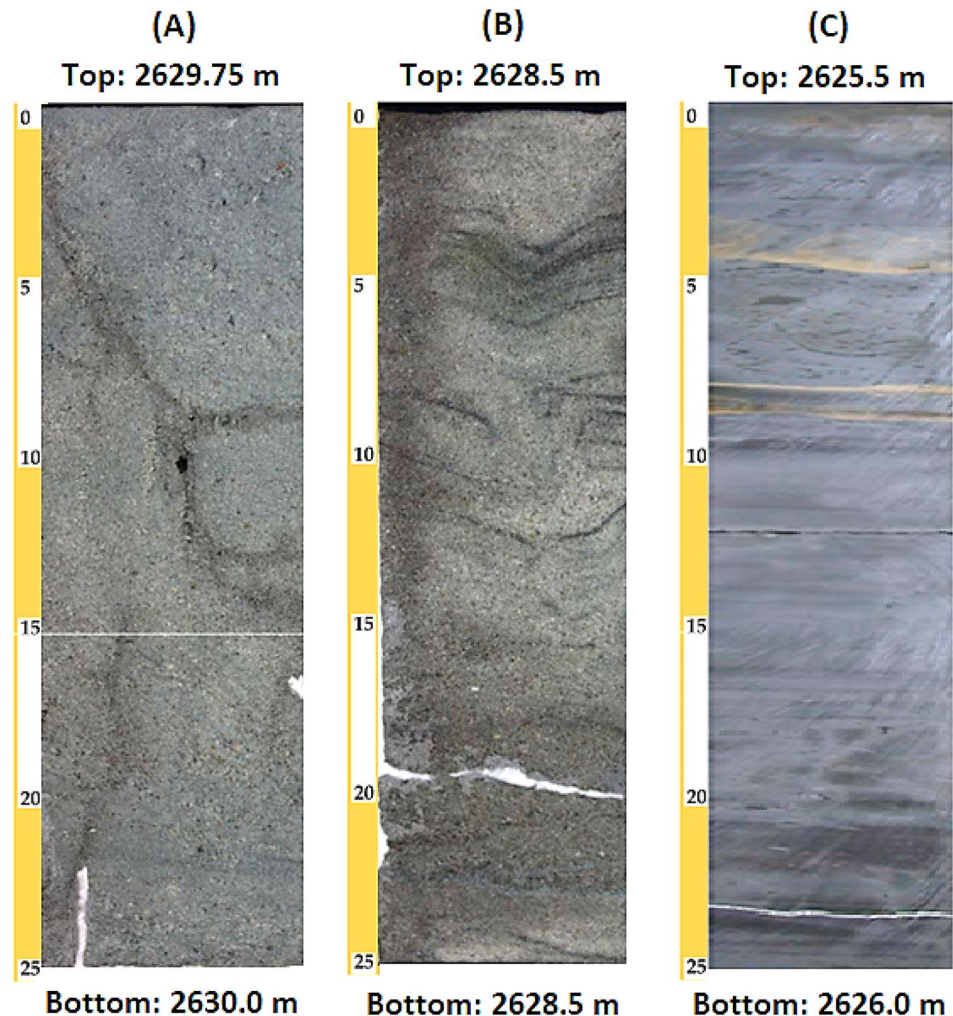
structures, slight lamination, dish structure (Fig. 4B), and dewatering structure (Fig. 4A). They are distributed along the whole interval as intercalated beds of variable thicknesses of gradational sequence.

These arenites are pebbly in most intervals, slightly argillaceous, poorly sorted, fine to medium-grained in most intervals, and locally coarse-grained with parallel lamination in parts and massive in parts. They are silty, pyretic, calcareous, and slightly cemented by variable calcite cement.

#### Mudstone lithofacies

Three mudstone lithofacies are recognized in the reservoir interval (1) laminated silty mudstone, (2) laminated sandy mudstone, and (3) deformed laminated silty mudstone (Fig. 4C). These muddy lithofacies dominate in the upper parts of the studied depth interval (2625–2628.2 m). They are moderate to dark gray, calcareous, sideritic, and ferruginous silty mudstone which is laminated and slightly deformed due to the bioturbation dominance.

**Fig. 4** Sedimentary structures and the lithofacies types of Abu Madi reservoir **A** dewatering structure of the mid- to outer-shelf deposits, **B** dish structure of mid- to outer-shelf deposits, and **C** laminated mud of tidal flat deposits





Less frequently, they are slightly deformed with some flasher laminations. Siderite and framboidal pyrite are scattered along different levels. They are interlaminated with some laminated arenites which are light gray to brownish gray.

### Petrographic characteristics

The grain size analysis using sieve analysis and the statistical processing of the obtained data indicates that the studied Abu Madi sandstone reservoir consists primarily of poorly sorted, medium to coarse sandstones (Fig. 5a, b). The petrographical examination of the available samples states the discrimination of the studied samples into 5 microfacies/lithofacies: (1) subfeldspathic arenite, (2) feldspathic arenite, (3) quartz arenites (bioclastic quartz arenite, lithic arenite, and quartz arenite), (4) quartz wacke, and (5) feldspathic quartz wacke. The arenite composition forms 90% of the total microfacies with a dominance of the quartz arenite microfacies (42 samples, 61%, Fig. 6). The assigned microfacies types are composed primarily of arenites that are described in detail as follows.

### Arenites composition

Petrographically, the arenite microfacies are the main microfacies recorded within the Abu Madi samples. Arenites represent 90% of the examined samples and 10% of the studied samples are wackes. They are mainly composed of poorly sorted, very fine to medium-grained, subrounded to angular, monocrystalline quartz grains, and rarely polycrystalline, with some plagioclase, K-feldspars, and subsidiary opaques, mica flakes, glauconite pellets, and rarely well-preserved bioclastic remains and lithic fragments. They are texturally immature and mineralogically sub-mature, especially in the feldspathic and subfeldspathic arenite microfacies. The arenite microfacies are described in detail as follows.

**Fig. 5** Frequency histograms of the average grain size (a) and the grain sorting (b) of the Abu Madi sandstone reservoir

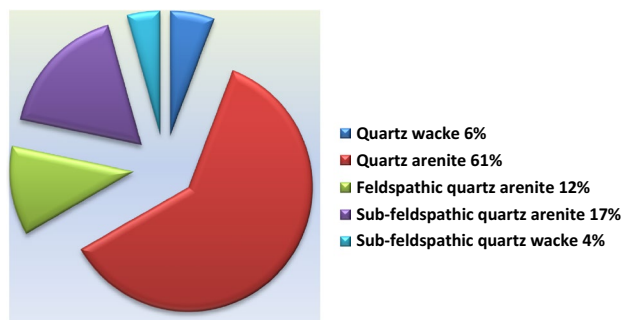
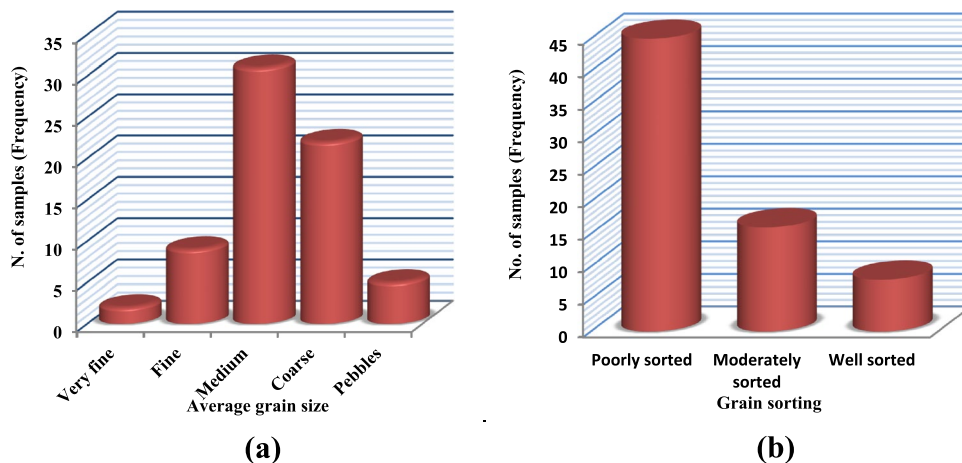


**Fig. 6** The exploded distribution pie of the microfacies types of the Abu Madi sandstone reservoir

### I. Subfeldspathic arenite microfacies

It is represented in the Abu Madi Formation at different levels (17%); it consists of poorly sorted very coarse to very fine, subrounded to subangular, and poorly cemented quartz grains, rarely with a few feldspar grains (Fig. 7a). The clastic grains are slightly compacted and cemented by calcite as meniscus cement. Compaction is represented by a grain-to-grain point and long contacts. The quartz grains are primarily monocrystalline and rarely polycrystalline. Microfractures are noticed in some grains, especially at their outer edges. Feldspars are represented by K-feldspars (microcline, Fig. 7a) and sometimes are altered. Also, carbonate rock fragments and fresh glauconite pellets are sometimes noticed (Fig. 7b), while cubic to sub-cubic framboidal pyrite are rarely noticed.

Pore spaces are primarily presented by (1) meso to micro-intergranular pore spaces (blue-dyed) and (2) microfractures within the clastic grains (Fig. 7b). The abundance of pore spaces gave rise to very good visual porosity values (25–27%).

### II. Quartz arenites microfacies

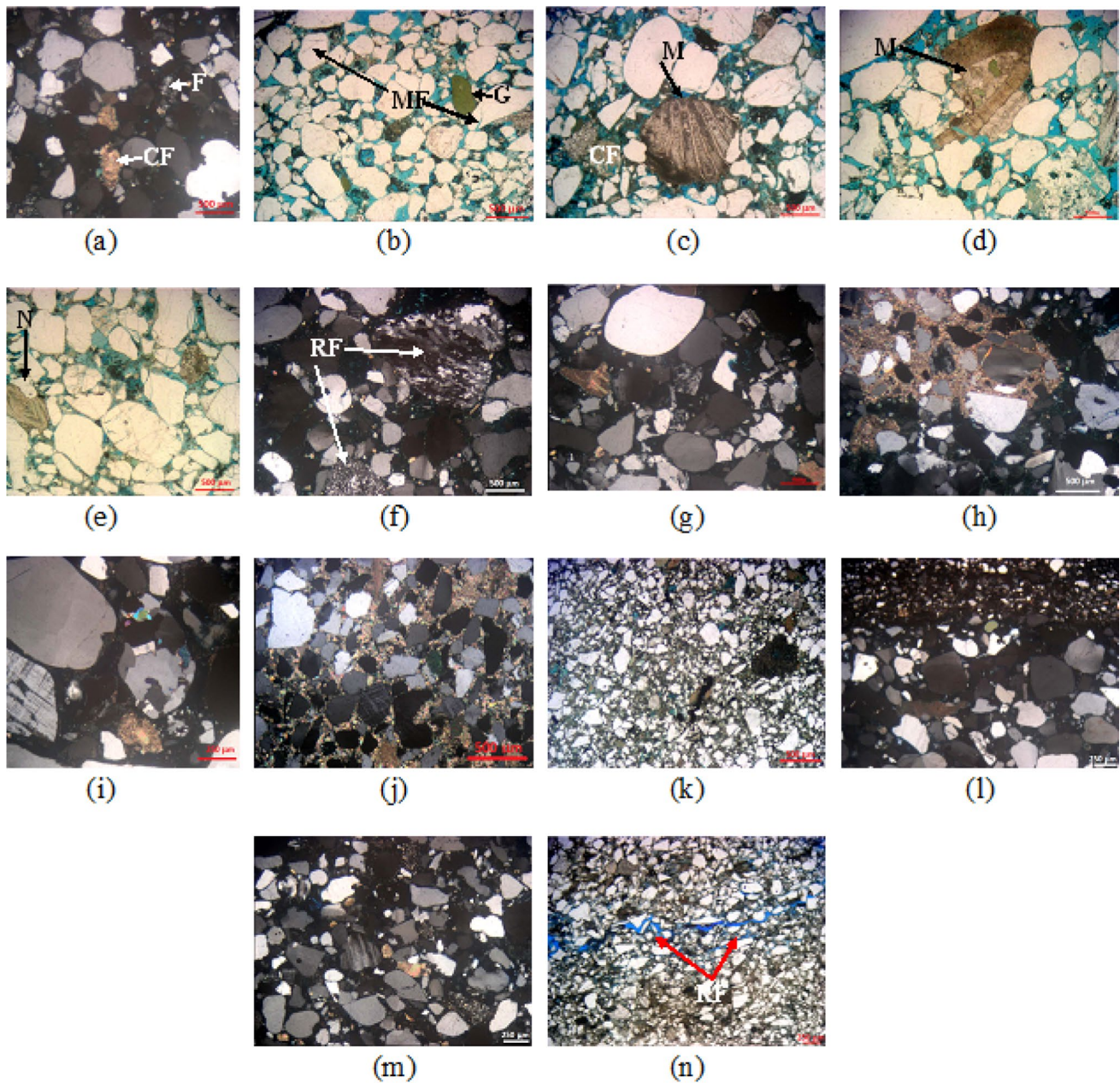


**Fig. 7** Photomicrographs of some microfacies types from S. Faraskur-3 well showing **a, b** subfeldspathic quartz arenite, depth 2818.16 m; **c–e** bioclastic quartz arenite, depth 2818.59 m; **f** lithic arenite, depth 2819.20 m; **g, h** quartz arenite, depth 2819.82 m; **i, j** feldspathic quartz arenite, depth 2822.56 m, 2825.76 m; **k** subfelds-

pathic quartz wacke, depth 2835.90 m; and **l–n** quartz wacke, depth 2631.47 m from S. Faraskur-4 well. Note F refers to the feldspars, MF microfractures, G glauconite pellets, CF carbonate fragments, M mollusca shells, N nummulite shells, RF rock fragments, and FR refers to the fractures

#### *Bioclastic quartz arenite*

It is primarily represented at the base of the Abu Madi reservoir; it consists of rounded to subangular, poorly sorted, and cemented very fine to pebbly sand-sized quartz grains with a few Mollusca shell fragments (Fig. 7c, d). Well-preserved nummulite shell fragments are also noticed in some samples (Fig. 7e).

The quartz grains are mostly monocrystalline, slightly cemented by calcite, and slightly compacted as long straight contacts with a few microfractures. The quartz grains are primarily monocrystalline; less frequently polycrystalline. Carbonate rock fragments, well-preserved glauconite pellets (Fig. 7d), and silt-sized framboidal pyrite grains are less frequently assigned (Fig. 7c). Visual porosity is very good

(23–26%) and presented by (1) meso- to microintergranular, blue-dyed pore spaces and (2) microfractures (Fig. 7c).

#### *Lithic arenite*

It is built of poorly sorted, fine to pebbly sized, subangular to rounded, and poorly cemented quartz grains (Fig. 7f); sometimes it is bioclastic with a few Mollusca content at different levels. The monocrystalline quartz grains are abundant; sometimes polycrystalline quartz grains are observed with some altered feldspars, glauconite pellets, and lithic fragments which are represented by micropolycrystalline quartz grains of igneous origin (Fig. 7f). The quartz grains are primarily monocrystalline; less frequently are polycrystalline. Compaction is presented by grain-to-grain points and long straight contacts (Fig. 7f). Visual porosity is very good (23–24%); it is presented by intergranular pore spaces.

#### *Quartz arenite*

This microfacies is predominant in the Abu Madi reservoir, where it constitutes 61% of the studied samples (Fig. 6). It is composed of abundant monocrystalline poorly sorted quartz grains which are very fine to pebbly sized, rounded to subangular, and friable (Fig. 7g). A few feldspars and carbonate rock fragments are also observed. The clastic grains are slightly compacted via point or long contacts (Fig. 7g). Visual porosity is very good to excellent and presented by meso- to microintergranular pore spaces (25%). Sometimes, it is highly cemented by calcite cement causing a reduction of the porosity values to 18% (Fig. 7h).

### III. Feldspathic arenite microfacies

The feldspathic arenite microfacies form about 12% of the studied Abu Madi samples (Fig. 6). It consists of monocrystalline, sometimes polycrystalline, poorly sorted, very fine-grained to coarse-grained, subangular to rounded, and friable quartz grains. K-feldspars in these microfacies are abundant; they are rounded to angular fine grains (Fig. 7i). Phenoclasts are poorly cemented by calcite and sometimes are highly cemented causing a high reduction in porosity values (Fig. 7j). The visual porosity values are very good to good and presented by microintergranular pore spaces (14–26%).

## Wacke composition

### I. Subfeldspathic quartz wacke microfacies

It is rarely represented in the Abu Madi reservoir (4%, Fig. 6). It consists of poorly sorted silty-sized to medium-grained quartz grains, subangular to subrounded, and friable (Fig. 7k). The quartz grains are monocrystalline to polycrystalline and moderately cemented by argillaceous material in which the grains are floating. K-feldspar grains and glauconite pellets are very fine to medium, mostly altered and floating within the argillaceous matrix. Furthermore, mica

flakes and rock fragments are rarely present. Pore spaces are primarily intergranular and highly reduced by clay-filling materials and iron oxides (10–13%, Fig. 7k).

### II. Quartz wacke

It is rarely represented in the Abu Madi reservoir (6%, Fig. 6); it is primarily represented by lamination between quartz wacke and quartz arenite bands (Fig. 7l). The wacke bands are composed of silt-sized quartz grains floating within a clayey matrix. The quartz grains are composed of mono- to polycrystalline, poorly sorted, fine to coarse, moderately sorted, well-rounded, and subangular grains compacted as long and point contacts, sometimes as concave–convex (Fig. 7m). K-feldspars are less frequently presented, while fine to very fine rounded carbonate rock fragments are also observed. The silt-sized quartz and feldspar grains are scattered in an argillaceous matrix with some fractures crossing the groundmass which improved the visual porosity (dyed-blue, Fig. 7n). The pore spaces are presented as (1) intergranular pore spaces, (2) matrix porosity, and (3) fractures. The visual porosity values vary between 12 and 19%.

## Clay fraction mineralogy

The XRD analysis is critically needed, as it provides the most efficient method for delineating the mineral composition of the clay fraction. The XRD data of the clay fraction of the subfeldspathic quartz arenite microfacies samples (RRT3) of the studied wells reveal that they are primarily composed of kaolinite (93–100%), sometimes with a few contents of illite (4%) and smectite/illite mixed layer (3%, Table 2). The quartz arenite microfacies (RRT1-2) is common in the S. Faraskur-4 well with less effective clay content is completely composed of kaolinite (100%), while the clay fraction of the feldspathic quartz arenite microfacies is characterized by low kaolinite content (29%) and relatively high illite (18%) and mixed smectite/illite (53%) fractions (Table 2). However, the implication of increasing the smectite/illite and illite fraction in the feldspathic quartz arenite microfacies is still slight in reducing permeability which is very good ( $k_H = 439$  md). On the other side, the clay fraction of the subfeldspathic quartz wacke microfacies (RRT2-4) and its relatively high smectite/illite mixed layer content (55–65%, Table 2) slightly reduced their permeability values (av.  $k = 73.2$  md).

## Diagenetic features

Diagenetic features are subdivided into two groups based on their implication on the reservoir porosity. They are divided into porosity-reducing and porosity-enhancing diagenetic features (Nabawy et al. 2020a, 2020b, 2022). For the Abu



Madi fluviomarine deposits, the porosity-enhancing features (dissolution and fracturing) are dominant, while the porosity-reducing features (cementation, compaction, and authigenic minerals) are minimized (Fig. 8). The visual porosity of the studied microfacies is primarily fair to very good ranging from 10 to 27%; the relatively high values are assigned to the quartz arenite, lithic quartz arenite, feldspathic quartz arenite, bioclastic quartz arenite, and the subfeldspathic quartz arenite microfacies. On the contrary, the lowest porosity values are encountered for the quartz wacke and the subfeldspathic quartz wacke microfacies.

### Porosity-enhancing diagenetic features

#### I. Dissolution

The studied shallow marine (tidal flat and mid- to outer-shelf settings) Abu Madi reservoir has been subjected to a significant dissolution and feldspars alteration, due to the impact of low Ca-bearing invading solutions. Dissolution of the cementing materials of the Abu Madi samples is mostly selective for a carbonate cement (Fig. 7b–e), while dissolution and alteration of feldspars are intensive (Fig. 7a, i) causing a relatively high improvement of the intergranular pore spaces. Dissolution is in charge of leaching the Mg-bearing calcite and the original aragonitic composition of the shell bodies which have a higher ability to be dissolved by relatively low Ca and Mg-bearing solutions (Boggs 2009; Nabawy et al. 2020a). The well-preserved shell bodies indicate that the coating of these shells by a

clay remnant protected them against dissolution as shown in the bioclastic arenite microfacies (Fig. 7c–e). However, dissolution is concerned only with the arenite microfacies. Dissolution of the quartz grains by low silica-bearing solutions is also noticed in some microfacies samples, e.g., the quartz wacke microfacies (Fig. 7l), and the quartz arenite microfacies (Fig. 7g). Furthermore, the glauconite pellets are sometimes highly weathered and dissected by some microcracks, e.g., the subfeldspathic arenite, (Fig. 7b), and the bioclastic quartz arenite microfacies (Fig. 7e). Dissolution of the original intergranular pore spaces improved the connectivity of these pore spaces and increased their sizes from micro- into mesopores (Fig. 7b–e).

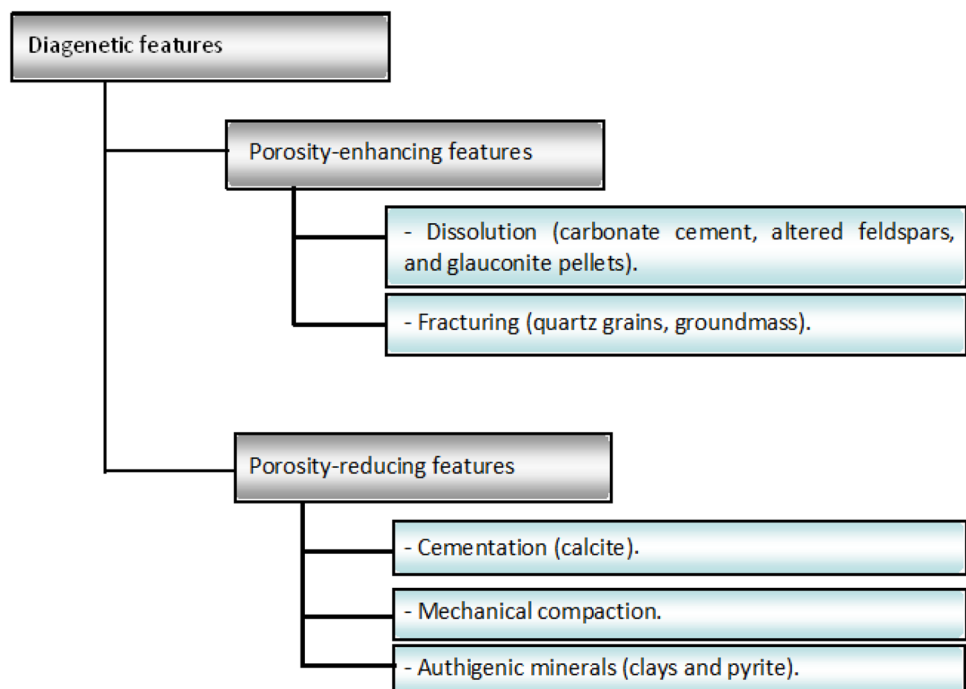
#### II. Fracturing

Fracturing is a rock failure due to the implication of predominated stresses affecting the reservoir quality. For the present study, stresses are delineated as microintersecting microfractures affecting the quartz grain bodies and edges, e.g., the subfeldspathic arenites (Fig. 7a, b) and the bioclastic arenites (Fig. 7c–e). The fracturing of the bioclastic remains may be prohibited by the early stages of coating by the argillaceous matrix (Fig. 7c–d). The groundmass of the wacke microfacies is intersected by open dyed-blue fractures which highly improved the reservoir quality of these microfacies, e.g., the quartz wacke microfacies (Fig. 7n).

### Porosity-reducing diagenetic features

#### I. Cementation

**Fig. 8** A sketch showing the main porosity-reducing and enhancing diagenetic features that predominated in the Abu Madi reservoir





Calcite cementation is the main diagenetic feature that controlled the Abu Madi reservoir; however, its implication is limited where most of the studied samples are friable with some gravity meniscus cement. It is represented by a few calcite patches between the quartz grains and the lithic fragments, e.g., subfeldspathic quartz arenite (Fig. 7a), and the quartz wacke (Fig. 7m), and the feldspathic quartz arenite microfacies (Fig. 7i). The presence of micro- and pseudosparite as pore-filling cement is rarely encountered, so its impact on reducing the pore connectivity is limited. Carbonate rock fragments are sometimes noticed as reworked materials, e.g., the quartz arenite microfacies (Fig. 7g), and the subfeldspathic quartz arenite microfacies (Fig. 7a). However, the predominance of the calcite cement is sometimes noticed as pervasive cement in which the quartz grains float, e.g., the quartz arenite (Fig. 7h) and the feldspathic quartz arenite (Fig. 7j). Predominance of the calcite cement reduced the visual porosity of some of these samples to 10% (Fig. 7h, j). The present calcite cement may be a relic of the original cement or may have originated later from re-precipitation of dissolved bioclastic remains and scattered carbonate lithic fragments (El-Ghali et al. 2013; Nabawy et al. 2020a). Also, the pervasive calcite cement may be originated as a result of invasion by phreatic meteoric water (Longman 1980).

Silica cement is rarely presented in the Abu Madi reservoir; however, the point contacts and pressure solution between the quartz grains may cause cementation by meniscus silica cement. Finally, cementation and pore filling by argillaceous materials is the result of clay minerals alteration not due to detrital clay content and will be discussed in the following section as authigenic minerals. However, early coating with thin films of clay minerals may be the main reason for protecting the well-preserved Mollusca and nummulite shell fragments against dissolution and leaching.

## II. Compaction

Mechanical compaction is among the main porosity-reducing diagenetic features that caused a reduction of the original intergranular pore spaces of the Abu Madi sandstone. It is started with initiating the burial process and its impact increases by increasing the burial depth (Chatalov and Stefanov 2014; Nabawy et al. 2022b). Tectonic stresses may be another source of this mechanical compaction which may be presented by some microcracks in the quartz grains and open fractures (Fig. 7b–e, n). The compaction stresses are indicated by the grain-to-grain point and long contacts which sometimes created microfractures along the border edges of the quartz grains (Fig. 7b, e). No indications are noticed for the presence of brittle or bent mica flakes. Due to the original high quality of the Abu Madi reservoir,

the reducing implication of the mechanical compaction is limited.

## III. Authigenic Minerals Content

Most of the Abu Madi samples are poorly cemented with minor traces of authigenic minerals. These are primarily represented by clay minerals, especially in the wacke microfacies, where clay patches are noticed as thin laminas alternated with sandstone bands (Figs. 4c, 7l). These clays are dominated by kaolinite, especially to the south of the study area in S. Faraskur-4 as well as revealed from the XRD analysis (Table 2). It is present as a pore-filling material that slightly deteriorates the pore connectivity, especially for the wacke microfacies. However, the visual porosity is still countable ( $\geq 10\%$ ). The kaolinite is associated with smectite/illite mixed layers (53–65%, Table 2), and illite clay (4–18%) minerals to the north of the study area in S. Faraskur-3 well. The smectite and illite occurrence appears at higher depths as revealed from the XRD data of the subfeldspathic quartz wacke microfacies and the feldspathic quartz arenite microfacies of the RRT2 samples (Table 2). Also, the authigenic minerals include a few patches of framboidal pyrite scattered within the groundmass between the feldspars and the quartz grains. The presence of pyrite (iron sulfides) indicates the dominance of a reducing depositional paleoenvironment. However, pyrite content seems to be in traces, so it is not indicated in the XRD analysis.

## Discussion

### Depositional environments

Deposition on the continental shelves (shelf, epeiric, neritic, and epicontinental) results in shallow-marine sedimentary deposits where the water depth is  $\leq 200$  m (James 1978; Lukasik et al. 2000; Leila et al. 2021). These shallow marine sediments are promising for hydrocarbon accumulation. Some shelves are vigorously stirred by tidal currents which are capable of moving sediment of almost all sizes. Gravity-driven density currents, produced by storms that cause vast quantities of sediment to be suspended, are important in some parts of the inner shelf. It has also become apparent that the internal waves within the water column can disturb the sediments of the outer shelves. From the description of the arenite lithofacies of the Abu Madi reservoir and their glauconitic and pebbles content, dewatering and dish structures indicate that the arenite facies were deposited in mid-to-outer-shelf siliciclastics affected by storm action.

On the other side, the laminated and blocky lenticular structures of some intervals with their calcareous, sideritic, and pyritic content, and their slight deformation by bioturbation are an indication of the deposition in a tidal flat

setting. Thereby, the lithofacies description indicates the deposition of the Abu Madi reservoir in a mid- to outer-shelf siliciclastic setting and less frequently in a tidal flat setting. From the petrographical data, the textural immature and the mineralogical sub-mature nature of the poorly sorted arenites, especially of the feldspathic and subfeldspathic arenite microfacies, indicate the deposition of these arenites in a high-energy environment, i.e., channel fills within a submarine tidal channel system.

### Effect of the mineralogical composition on the reservoir properties

The studied Abu Madi microfacies are of a clastic nature and can be discriminated into arenites and wackes with more clay dominance in the wacke microfacies. This clay content reduced the reservoir properties and quality of these wacke streaks (RRT4 samples) into tight to poor reservoir quality, while the reservoir quality of most RRT3 samples (quartz wacke, subfeldspathic quartz wacke, and subfeldspathic quartz arenite microfacies) was reduced into fair quality (Fig. 7b). However, the moderate impact of increasing the clay content in the wacke types may indicate that the clay fraction is mostly represented by ineffective structural detrital clay scattered within the cement/matrix. Kaolinite forms the main clay content of most samples in the Abu Madi reservoir, and the illite clay fractions are products of chemical and physical weathering and are thereby considered of detrital origin. On the contrary, the smectite/illite mixed layers are formed in diagenetic environments due to the alteration of smectite.

Also, kaolinite is less frequently formed due to the alteration of the feldspar content in the feldspathic microfacies, i.e., it is represented by authigenic dispersed clays. Thereby, the clay fraction of the Abu Madi reservoir, especially of the feldspathic and subfeldspathic quartz wacke microfacies, may represent a balanced midway state between the detrital depositional origin and the authigenic fractions due to the feldspars alteration. The predominance of the mixed layer and kaolinite in the studied microfacies indicates a marine origin for these clay mineral associations. This balanced midway origin of the clay fraction reduced its implication on the reservoir wacke microfacies which is still prospective with fair to good permeability for the RRT3 and RRT4 samples (av.  $k_H = 169.1$  and  $6.87$  md, respectively, Table 1). Another explanation of the slight impact of the kaolinite content on the Abu Madi reservoir may be attributed to the leaching out of most of this clay content due to invasion by a high flow rate of fluids. This explanation may be supported by the relatively wide pore throats of the arenite microfacies of the RRT1 and RRT2 groups (macropore sizes  $\geq 10$   $\mu\text{m}$ , Table 1).

### Implication of porosity and lithology on density

Bulk density ( $\rho_b$ ) is a resultant vector of the grain density ( $\rho_g$ ) and pore volume percentage ( $\emptyset$ ) as mentioned by some researchers (e.g., Teama and Nabawy 2016, 2018; Khater et al. 2020; Kassem et al. 2022). So, plotting  $\rho_b$  versus  $\rho_g$  states that the lithology of the Abu Madi reservoir is dominated by the sandstone composition ( $\rho_g$  of quartz =  $2.65$  g/cm<sup>3</sup>, Fig. 9).

Shifting some samples into higher grain density values is due to the relatively high iron oxides and sulfides content, whereas shifting to relatively low values, in particular of the RRT3 and RRT4 samples (subfeldspathic quartz wacke composition), is due to their relatively high argillaceous content (quartz wacke and subfeldspathic quartz wacke microfacies). These two microfacies are also characterized by the highest bulk density due to the influence of the reducing-porosity diagenetic features on the pore volume. Presenting  $\rho_b$  versus  $\emptyset$  which is frequently applied as a quality control plot for the core data values (Nabawy 2018) shows a set of high-reliability best-fit lines ( $R^2 \geq 0.908$ , Fig. 10) with the highest porosity assigned for the RRT1 and the RRT2 which consists of (feldspathic quartz arenite, subfeldspathic quartz arenite, and quartz arenites).

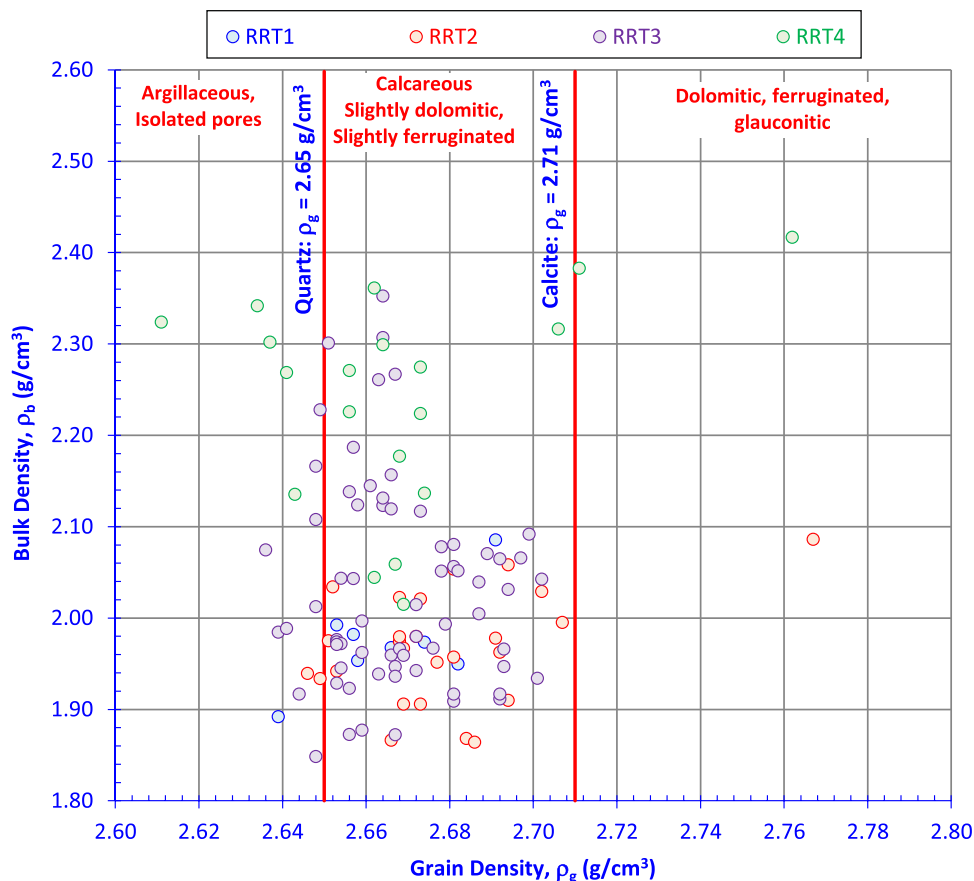
Shifting the constant value ( $\rho_g$ ) of the RRT3 and RRT4 models to higher values ( $2.70$ – $2.77$  g/cc) is attributed to the presence of pyrite. The porosity ( $\emptyset_{He}$ ) of the Abu Madi clastic reservoir could be estimated using  $\rho_b$  as follows.

$$\rho_b(\text{g/cc}) = -0.026\emptyset_{He} + 2.66 \quad (R^2 = 0.984) \quad (7)$$

### Permeability (k) attributes

Permeability represents the capability of the reservoir to transmit the stored fluids, so it is primarily attributed to porosity and  $R_{35}$ . Therefore, plotting  $k$  versus  $\emptyset$  is the master plot for dividing the reservoir rock samples into groups based on their abilities to store and deliver fluids. This plot is preferred to be integrated with the DRT values as an indicator of the reservoir quality (Shenawi et al. 2007). For the Abu Madi samples, applying this plot indicates that they should be grouped into four RRTs each with its unique DRT range (Fig. 11a). Using 5% porosity and 1.0 md as cutoff values for the Faraskur gas reservoir reveals that all samples are prospective, i.e., located in the first quarter of the plot with prospective porosity and permeability values. A wide range for porosity is indicated for both RRT3 and RRT4 (10–30%, fair to excellent values), while very good to excellent values are assigned to the RRT1-2 which is attributed to their dominated arenite composition (Fig. 11a). Consequently, the permeability of the RRTs 1–2 and some of the

**Fig. 9** Plotting the bulk density versus the grain density of the Abu Madi Formation, S Faraskur-3 well, Nile Delta of Egypt



RRT3 are distinguished by very good to excellent  $k$  values ( $k \geq 1000$  md, Fig. 11a) due to the dominance of the arenite composition. The permeability of the studied RRTs can be estimated in terms of porosity using the following models.

$$\text{RRT1} : k = 2 \times 10^{-5} \phi_{\text{He}}^{5.69} \quad (14.6 \leq \text{DRT} \leq 15.0) \quad (R^2 = 0.984) \quad (8)$$

$$\text{RRT2} : k = 6 \times 10^{-7} \phi_{\text{He}}^{6.40} \quad (13.0 \leq \text{DRT} \leq 14.5) \quad (R^2 = 0.655) \quad (9)$$

$$\text{RRT3} : k = 1 \times 10^{-5} \phi_{\text{He}}^{4.99} \quad (11.0 \leq \text{DRT} \leq 12.9) \quad (R^2 = 0.775) \quad (10)$$

$$\text{RRT4} : k = 4 \times 10^{-4} \phi_{\text{He}}^{3.37} \quad (9.7 \leq \text{DRT} \leq 10.9) \quad (R^2 = 0.894) \quad (11)$$

Superimposing the FZI lines on the  $\phi$ - $k$  plot indicates the RRT1-2 samples are distinguished by  $\text{FZI} \geq 3.40 \mu\text{m}$  (Fig. 11b), i.e., having fair reservoir quality (Nabawy et al. 2015; Nabawy and El Sharawy 2018). On the contrary, the RRT4 has tight quality ( $\text{FZI} < 1.19 \mu\text{m}$ , Fig. 11b).

Even though porosity is a main contributor to permeability, it is primarily based on  $R_{35}$  values as a prime attributor, while its dependence on porosity is a subsidiary (Nabawy 2018; Radwan et al. 2022b; Nabawy et al. 2022b). Thereby,

plotting  $k$  versus  $R_{35}$  states that  $R_{35}$  is the prime attribute to  $k$  with very high reliability ( $R_{35} \geq 0.954$ , Fig. 12) of the obtained best-fit lines' models.

$$\text{RRT1} : R_{35} = 1.90 \phi_{\text{He}}^{2.07} \quad (R^2 = 0.981) \quad (12)$$

$$\text{RRT2} : R_{35} = 3.31 \phi_{\text{He}}^{1.97} \quad (R^2 = 0.984) \quad (13)$$

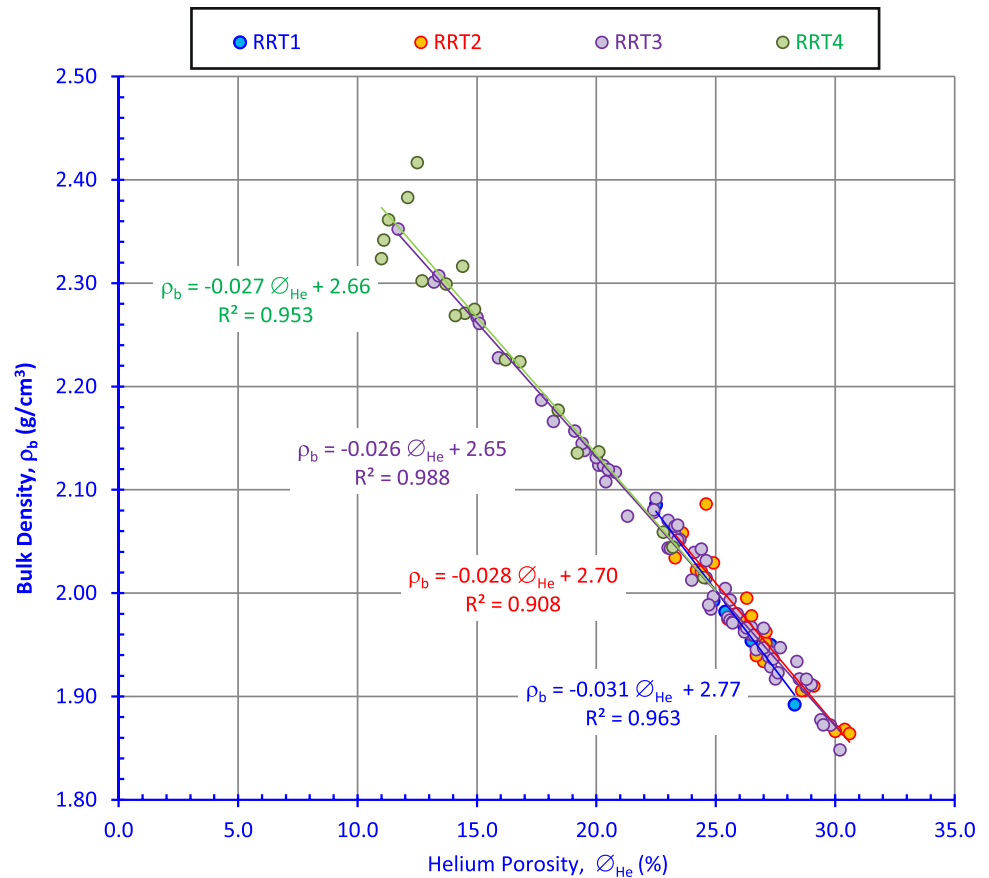
$$\text{RRT3} : R_{35} = 2.74 \phi_{\text{He}}^{2.15} \quad (R^2 = 0.976) \quad (14)$$

$$\text{RRT1} : R_{35} = 2.75 \phi_{\text{He}}^{2.66} \quad (R^2 = 0.954) \quad (15)$$

### Permeability anisotropy ( $\lambda_k$ )

Permeability anisotropy ( $\lambda_k$ ) refers to the ratio between  $k_H$  and  $k_V$  at the same depth level. As mentioned by Nabawy et al. (2015), depositional/primary fabrics are characterized by higher  $k_H$  than  $k_V$  which is commonly present. On the other side, the state of  $k_V > k_H$  is an indication for prevailing the secondary fabrics due to the prevalence of some vertical microfractures in the studied plugs as the case of some RRT3-4 wacke samples than the arenite samples (Fig. 13a).

**Fig. 10** Plotting the bulk density as a function of the core porosity of the Abu Madi Formation, S Faraskur-3 well, Nile Delta of Egypt



These vertical microfractures are primarily due to the implementation of the overload pressure. For ranking the anisotropy values based on the reservoir quality classification ranks of Nabawy et al. (2015), the  $k_H$ – $k_V$  plot is superimposed by the anisotropy ( $\lambda$ ) ranks (Fig. 13b). It is indicated that though characterizing some RRT3–4 wacke sample by highly and moderately secondary fabrics, they are dominated by highly and moderately depositional fabrics due to their main argillaceous composition as revealed from the petrographical study. A few RRT1–2 arenite samples have highly or moderately primary fabrics. This may be due to the presence of slight clay content and increasing the implication of the compaction effect as stated from the petrography (Fig. 7a–c, f–g).

### Reservoir quality attributes

The term reservoir quality refers to the capability of the reservoir to store and deliver hydrocarbons, so it is primarily attributed to porosity and permeability. Therefore, the FZI and RQI quality parameters are presented against  $\phi$  to check their contribution to the reservoir quality (Fig. 14a). It is indicated that the porosity of the RRT1–3 slightly contributes to the RQI of these RRTs ( $0.575 \leq R^2 \leq 0.691$ ), while the RQI of the RRT4 samples is moderately

attributed to their porosity ( $R^2 = 0.806$ ). Concerning the FZI, statistically and based on the FZI– $\phi$  plot, it is not dependent on porosity where data of the RRTs samples are highly scattered (Fig. 14b). However, theoretically FZI is dependent on both the RQI and the NPI which are based on  $\phi$ . This is explained by shifting and scattering the FZI– $\phi$  data due to the implication of the NPI values which is based on the pore/grain volume ratio; therefore, it is shifted due to the grain volume impact (Nabawy et al. 2015, 2020a, b, c).

Thereby, the weak to moderate dependence of the reservoir quality parameters on the porosity is due to their main dependence on the permeability ( $k$ ). Plotting the RQI and FZI against  $k$  indicates that  $k$  is the main attributor of these parameters (Fig. 15a, b), where some extremely reliable mathematical equations are estimated for the RQI– $k$  values ( $R^2 \geq 0.985$ , Fig. 15a).

The RQI values of all RRTs can be estimated with very high precision based on  $k$  using the following model.

$$\text{RRTs} : R_{35} = 0.086k^{0.445} \quad (R^2 = 0.995) \quad (16)$$

Despite the dependence of the RQI on permeability ( $k$ ), the dependence of the FZI on  $k$  is slightly scattered ( $0.833 \geq R^2 \geq 0.703$ , Fig. 15b). No best-fit line can be



**Fig. 11** Rock typing based on the permeability–porosity plot (a). The same plot is superimposed by the flow zone indicator values (b) as a tool for dividing the reservoir into flow units. The plot is supported by the porosity and permeability classification ranks (Nabawy 2018; Elgendy et al. 2020; El Sawy et al. 2020)

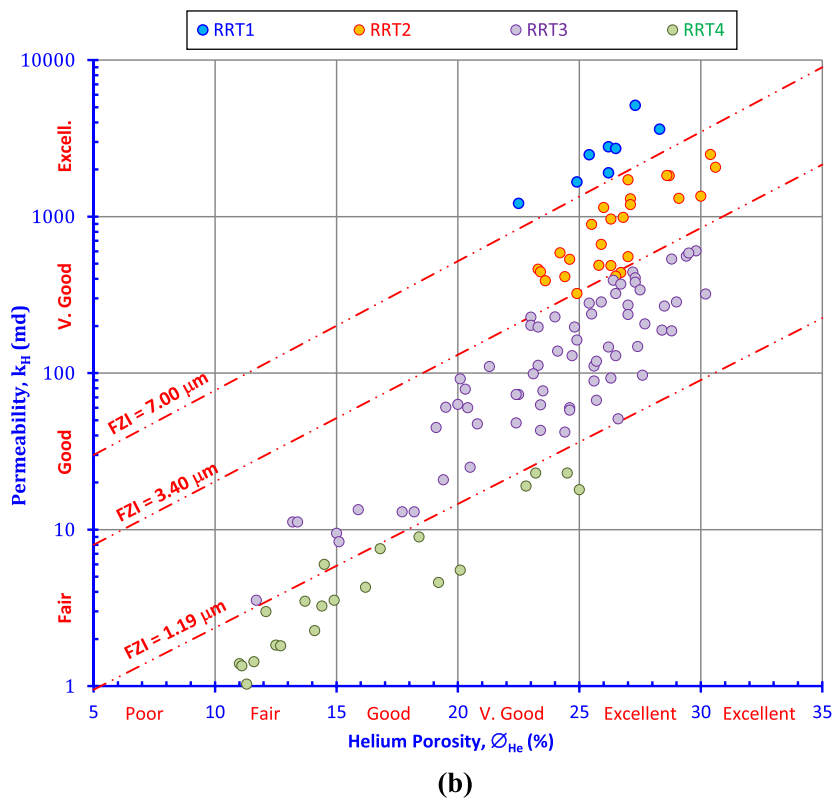
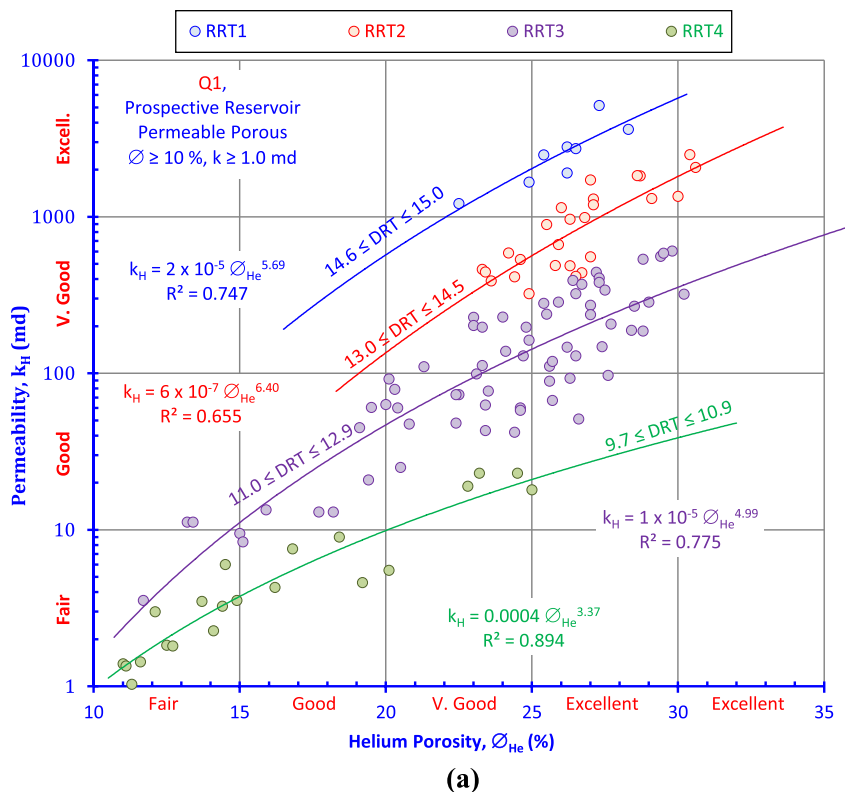
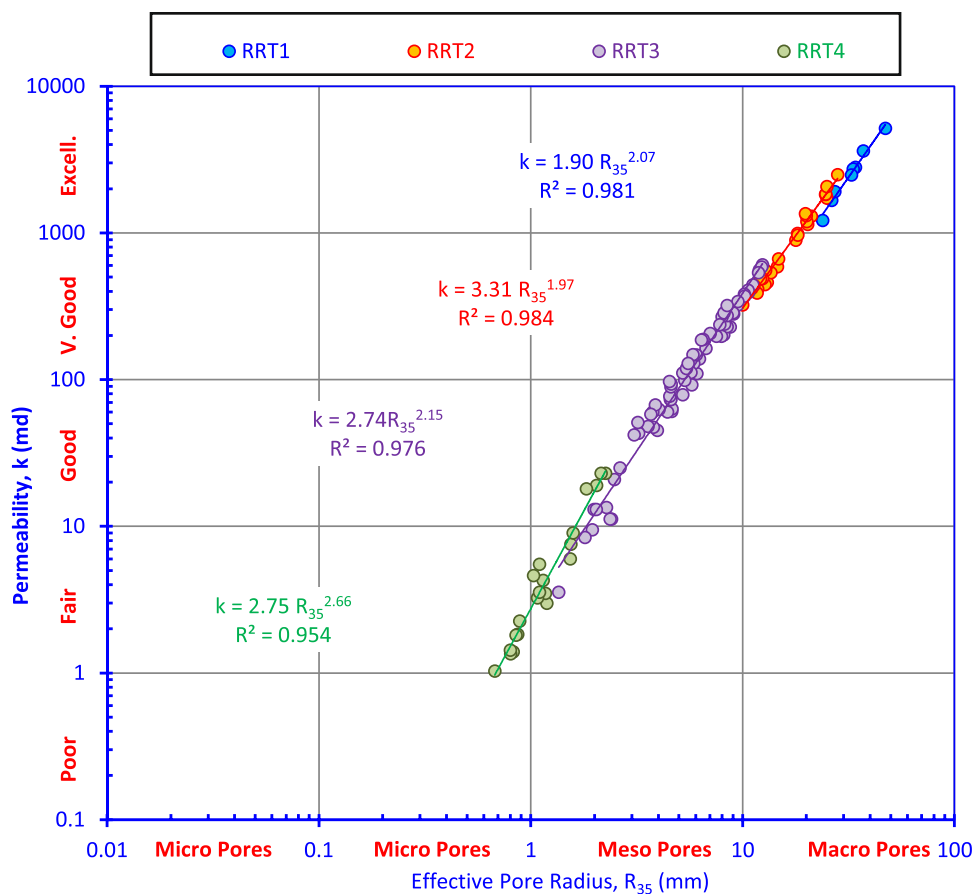


**Fig. 12** Plotting the permeability as a function of the effective pore radius  $R_{35}$  of Winland (1972). The plot is supported by the  $R_{35}$  classification ranks of Nabawy (2018)



assigned for the wacke RRT4 samples ( $R^2 = 0.085$ ) which may be attributed to their high argillaceous content.

### Reservoir quality ranks

Rock typing and reservoir quality ranking are among the main challenges of the reservoir characterization process which is primarily based on the reservoir storage and deliverability capacities. So, plotting the RQI-NPI plot is used to check the success of the rock typing process. This plot indicates that applying the rock typing process to the Abu Madi RRTs is successful and that their data samples are discriminated by three FZI lines of unique values (FZI = 7.0, 3.4., and 1.19  $\mu\text{m}$ , Fig. 16a). The line of FZI = 3.4  $\mu\text{m}$  is a diagnostic line separating the RRT1-2 arenite samples and the RRT3-4 wacke samples. Besides that, the RQI-FZI plot is applied to rank the reservoir quality (Fig. 16b). It is indicated that the RRT1-2 arenites have good to very good RQI and fair to very good FZI. The quartz wacke and the sub-feldspathic quartz wacke RRT4 samples have tight to poor quality, while the RRT3 samples are considered transitional between the RRT4 and RRT1-2 samples. The tightness and poor quality of some RRT3-4 samples are attributed to the

compaction process, cementation, and the argillaceous content as indicated from the petrographical studies.

### Conclusions

Integrating the sedimentological and petrophysical studies is applied in the present study to declare the implication of the lithofacies types and diagenesis on the Abu Madi reservoir in Faraskur Gas Field. To achieve this target the petrophysical rock typing is applied successfully based on the porosity, permeability, and DRT values and then interpreted in terms of the microfacies type and predominant diagenetic features.

The outputs of the present study can be summarized as:

- Sedimentological and petrographical studies of the Abu Madi reservoir in Faraskur Field indicate that the studied reservoir possesses five microfacies types as follows: quartz arenite, quartz wacke, feldspathic quartz arenite, sub-feldspathic quartz arenite, and sub-feldspathic quartz wacke.
- The arenite lithotypes description indicates the deposition of the Abu Madi reservoir in a mid- to outer-shelf

**Fig. 13** Discriminating the studied samples into samples having secondary and depositional fabrics (a) and b ranking the anisotropy of these samples based on its  $k_H-k_V$  plot b support by the anisotropy ranks classification of Nabawy (2018) and Nabawy et al. (2015, 2020b)

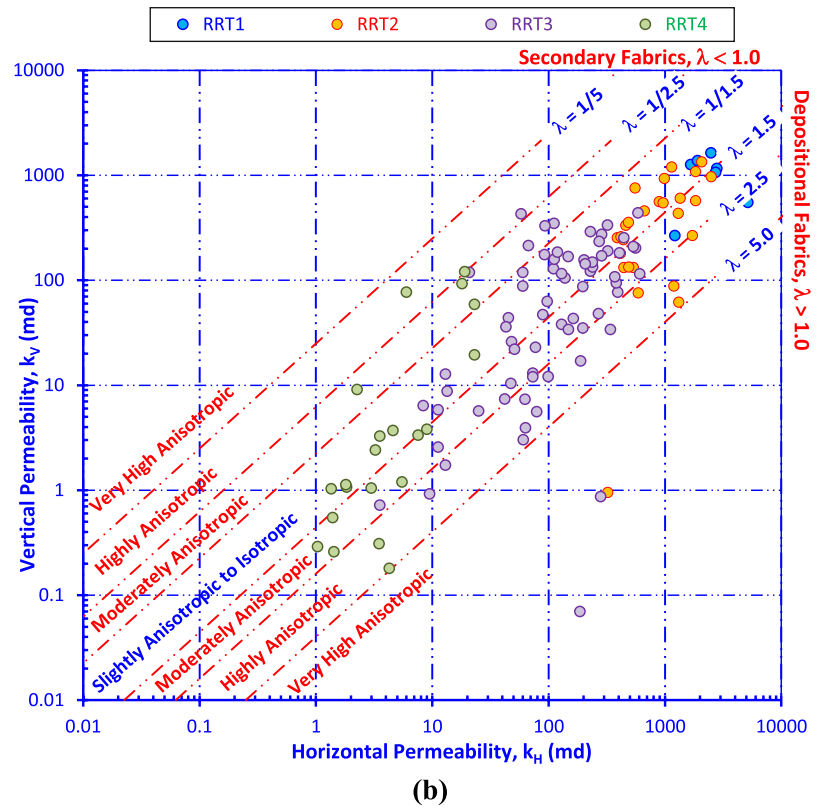
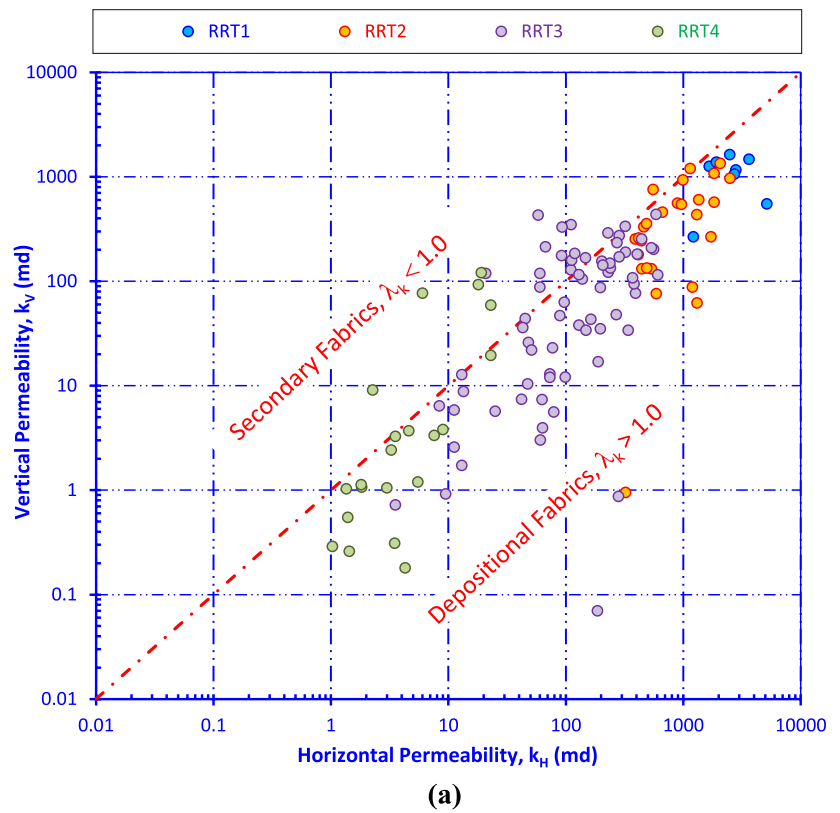


**Fig. 14** Plotting the porosity ( $\phi_{He}$ ) versus: **a** the reservoir quality index (RQI) and **b** the flow zone indicator (FZI). It is supported by the reservoir quality classification ranks (Nabawy et al. 2020a, b, c; Abuamarah and Nabawy 2021; Safa et al. 2021)

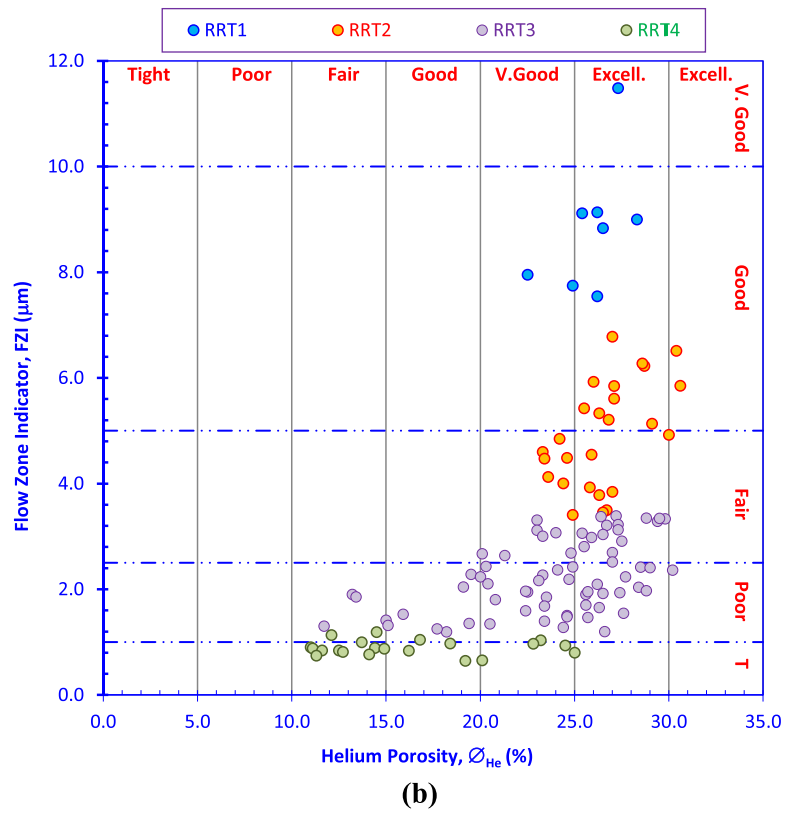
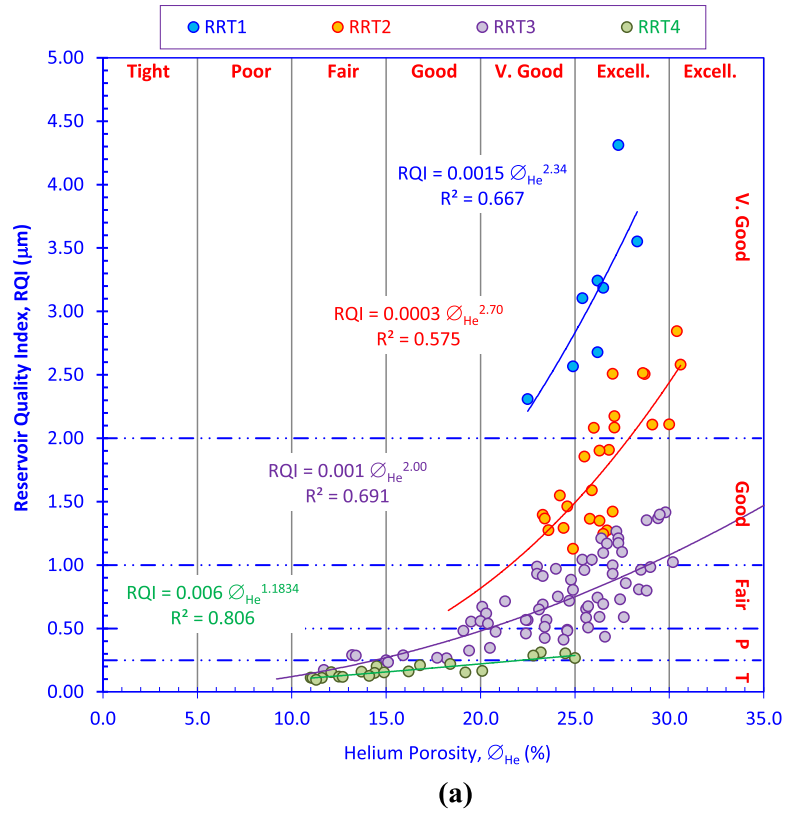




**Fig. 15** Plotting the permeability ( $k_H$ ) versus: **a** the reservoir quality index (RQI) and **b** the flow zone indicator (FZI) supported by the classification ranks of the flow zone indicator (Nabawy et al. 2020a, b, c; Abuamarah and Nabawy 2021; Fea et al. 2022)

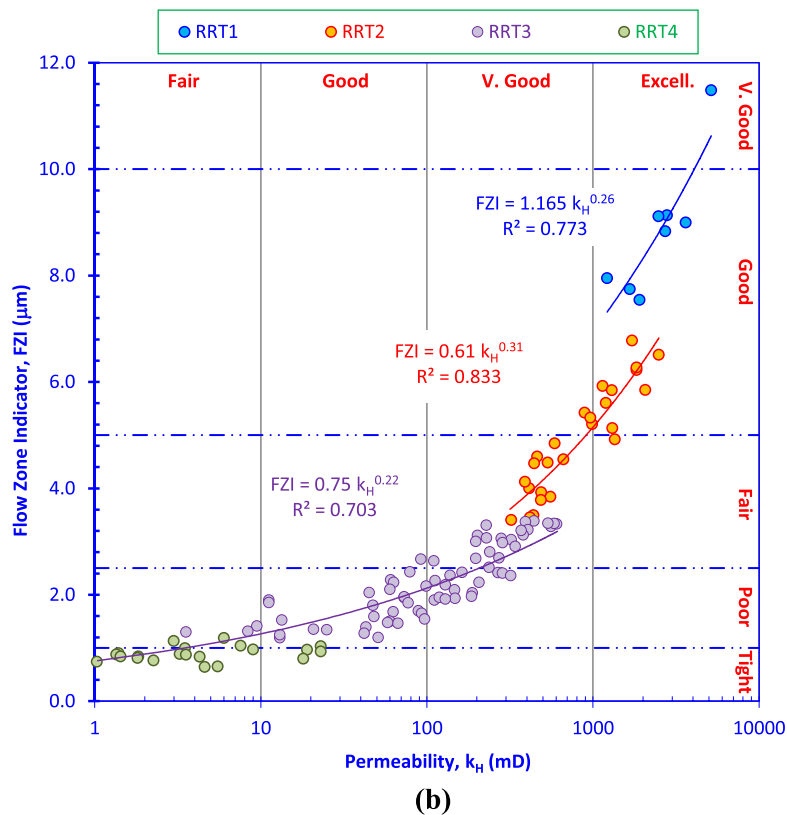
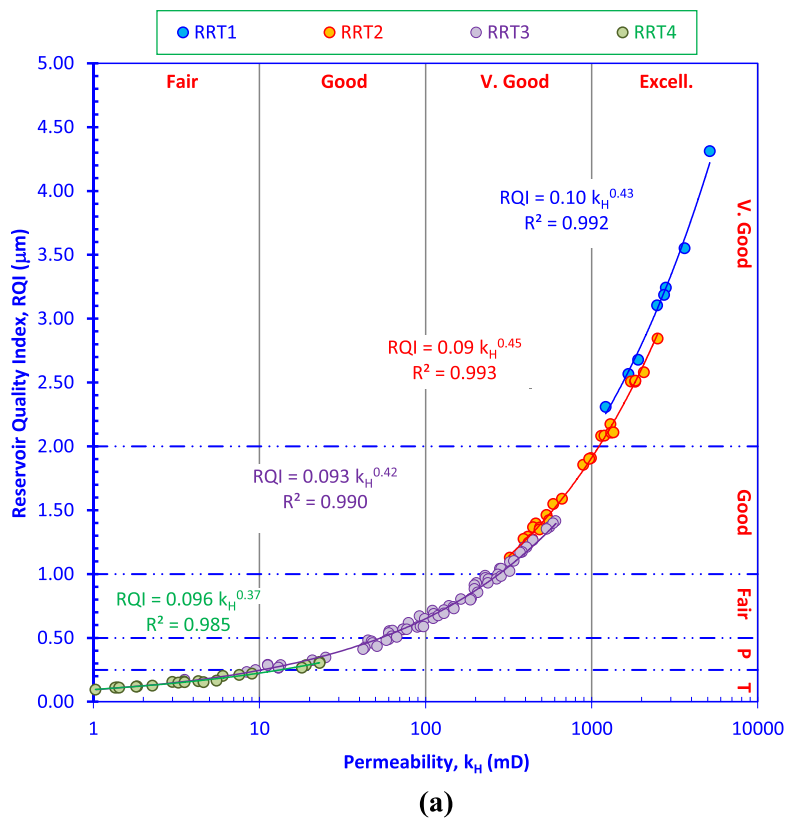
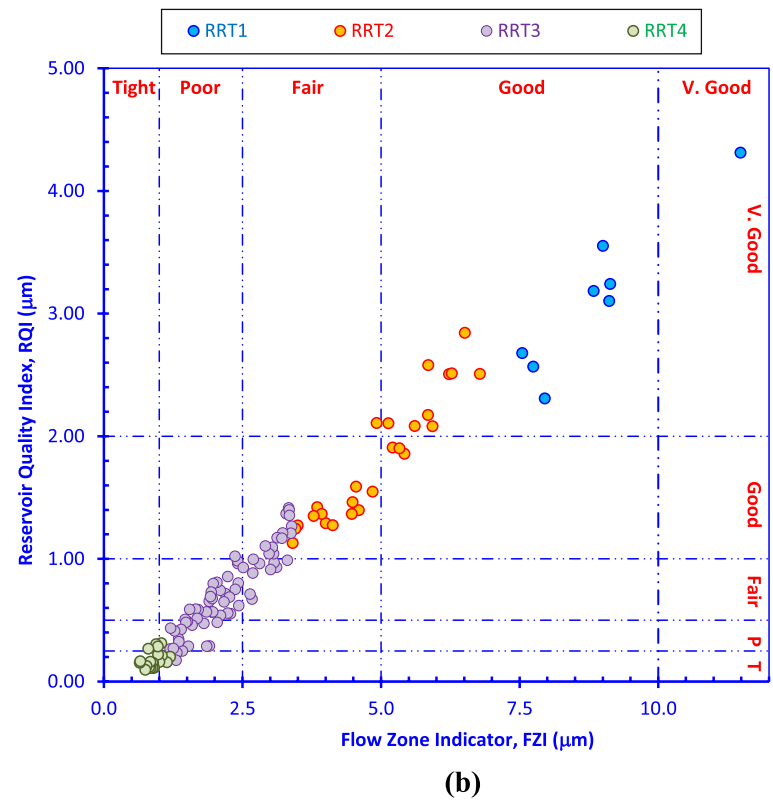
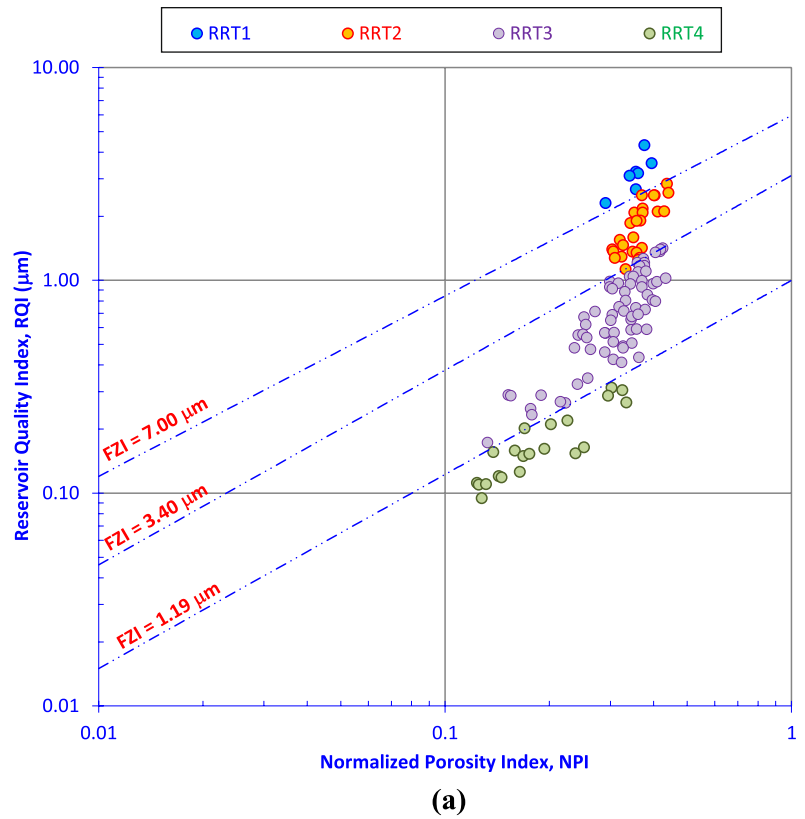


**Fig. 16** Plotting the reservoir quality index (RQI) against its main attributes: **a** normalized porosity index (NPI) and **b** flow zone indicator. It is applied as a tool for ranking the reservoir quality following the classification ranks of Nabawy (2018) and Nabawy et al. (2020a)



siliciclastic setting and less frequently in a tidal flat setting.

- The petrographical data, textural parameters, and the mineralogical sub-mature nature indicate the deposition of these arenites in a high-energy environment.
- Petrographically, the Abu Madi reservoir is composed of medium-grained quartz cemented calcite and iron oxides, clays (smectite/illite mixed layers and sometimes kaolinite), and pyrite.
- The primary intergranular porosity is dominated by some subordinate fractures and dissolution pore spaces.
- Cementation affected the reservoir quality by reducing the permeability and the macroporosity of the quartz wacke (reservoir rock type-4, RRT4).
- Petrophysically, the normalized porosity index (NPI), reservoir quality index (RQI), flow zone indicator (FZI), and the effective pore radius of Winland ( $R_{35}$ ) are used for ranking the reservoir quality of the Abu Madi sandstones which are grouped into four RRTs.
- The RRT1 (quartz arenite microfacies) has the highest petrophysical and reservoir quality parameters (av.  $\emptyset = 25.9\%$ , av.  $k_H = 2695$  md, av. DRT = 14.9, av. RQI = 3.12  $\mu\text{m}$ , av. FZI = 8.85  $\mu\text{m}$ , av.  $R_{35} = 32.7$   $\mu\text{m}$ ).
- The RRT4 group (quartz wacke, feldspathic quartz arenite, and subfeldspathic quartz wacke microfacies) has the lowest  $k$  and  $\emptyset$  values (av.  $\emptyset = 16.2\%$ , av.  $k_H = 6.87$  md) and the lowest reservoir quality parameters (av. DRT = 10.4, av. RQI = 0.18  $\mu\text{m}$ , av. FZI = 0.89  $\mu\text{m}$ , av.  $R_{35} = 1.26$   $\mu\text{m}$ ).
- Finally, the RRT2 and the RRT3 (quartz wacke, quartz arenite, feldspathic quartz arenite, subfeldspathic quartz arenite, and subfeldspathic quartz wacke microfacies) are considered transitional groups (av. DRT = 13.8 and 12.1, respectively) characterized by midway reservoir quality and petrophysical parameters between the RRT1 and the RRT4 samples. The permeability anisotropy of these two RRTs is the highest in the Faraskur Field (av.  $\lambda_k = 2.4$  and 2.62, respectively).

**Funding** Open access funding provided by The Science, Technology & Innovation Funding Authority (STDF) in cooperation with The Egyptian Knowledge Bank (EKB).

## Declarations

**Conflict of interest** The authors do not have any conflict of interest to disclose.

**Open Access** This article is licensed under a Creative Commons Attribution 4.0 International License, which permits use, sharing, adaptation, distribution and reproduction in any medium or format, as long as you give appropriate credit to the original author(s) and the source,

provide a link to the Creative Commons licence, and indicate if changes were made. The images or other third party material in this article are included in the article's Creative Commons licence, unless indicated otherwise in a credit line to the material. If material is not included in the article's Creative Commons licence and your intended use is not permitted by statutory regulation or exceeds the permitted use, you will need to obtain permission directly from the copyright holder. To view a copy of this licence, visit <http://creativecommons.org/licenses/by/4.0/>.

## References

- Abd El-Gawad EA, Abdelwahhab MA, Bekiet MH, Noah AZ, ElSayed NA, Fouda AEE (2019) Static reservoir modeling of El Wastani Formation, for justifying development plans, using 2D seismic and well log data in Scarab field, offshore Nile Delta Egypt. *J Afr Earth Sci* 158:103546
- Abd-Allah AMA, Abdel Aal MH, Ghandour A (2012) Structural characteristics and tectonic evolution of the northwestern margin of the Nile Delta, Egypt. *J Afr Earth Sci* 68:82–95
- Abdeen MM, Ramadan FS, Nabawy BS, El Saadawy O (2021) Sub-surface structural setting and hydrocarbon potentiality of the Komombo and Nuqra Basins, South Egypt: a seismic and petrophysical integrated study. *Nat Resour Res* 30(5):3575–3603
- Abdel Aal A, Price RJ, Vaitl JD, Shallow JA (1994) Tectonic evaluation of the Nile Delta, its impact on sedimentation and hydrocarbon potential. 12th EGPC Expl. Prod. Conf. Cairo, Egypt 1:19–34
- Abdel-Fattah MI (2014) Petrophysical characteristics of the Messinian Abu Madi Formation in the Baltim east and north fields, offshore Nile delta. *Egypt J Petrol Geol* 37(2):183–195
- Abed AA (2014) Hydraulic flow units and permeability prediction in a carbonate reservoir, southern Iraq from well log data using non-parametric correlation. *Int J Enhanc Res Sci Technol Eng* 3(1):480–486
- Abu El Ata AS, Ghoneimi AE, Azzam SS, (1999) Seismic stratigraphic analysis of the Nile Delta of Egypt. As concluded from seismic reflection interpretation. *Proc. 1st International Symp. Geoph., Tanta*, 158–173.
- Abu El-Ella R (1990) The Neogene-quadernary section in the Nile delta, Egypt: geology and hydrocarbon potential. *J Petrol Geol* 13(3):329–340
- Abuamarah BA, Nabawy BS (2021) A proposed classification for the reservoir quality assessment of hydrocarbon-bearing sandstone and carbonate reservoirs: a correlative study based on different assessment petrophysical procedures. *J Natl Gas Sci Eng* 88:103807
- Abuhagaza AA, El Sawy MZ, Nabawy BS (2021) Integrated petrophysical and petrographical studies for characterization of reservoirs: a case study of Muglad Basin, North Sudan. *Environ Earth Sci* 80(5):171
- Amaefule JO, Altunbay M, Tiab D, Kersey DG, Keelan DK (1993). Enhanced reservoir description: using core and log data to identify hydraulic (flow) units and predict permeability in uncored intervals/wells. SPE 26436. Paper presented at the SPE annual technical conference and exhibition, Houston, Texas, 3–6.
- Ashoor R, Nabawy BS, Kamel A (2023) Formation evaluation and reservoir quality assessment of the Albian clastic sequence in the SWM Oilfield, Southwest the Mesopotamian Basin, Iraq. *J Petrol Explor Prod Technol* 13:553–576
- Barakat MG (1982) General review of the petroliferous provinces of Egypt with special emphasis on their geological setting and oil potentialities, development research and technological planning center. Cairo Univ, Cairo, p 96
- Barakat MKh (2010) Modern geophysical techniques for constructing a 3D geological model on the Nile Delta Egypt Dissertation. The

- Technical University of Berlin. <https://doi.org/10.14279/depos-2627>
- Barakat M, Dominik W (2010) Seismic Studies on the Messinian Rocks in the Onshore Nile Delta, Egypt. 72nd Eur Assoc Geosci Eng Conf Exhib 2010 A New Spring Geosci Inc SPE Eur 2010 7: cp-161–00770. <https://doi.org/10.3997/2214-4609.201401362>
- Barber PM (1981) Messinian sub-aerial erosion of the proto Nile Delta. *Marine Geol* 44:253–272
- Bigdeli A, Delshad M (2023) Strategy for Optimum Chemical Enhanced Oil Recovery Field Operation. *Journal of Resource Recovery* 1:1001
- Boggs S (2009) *Petrology of sedimentary rocks*, 2nd edn. Cambridge University Press, New York, p 600
- Chatalov A, Stefanov Y (2014) Diagenesis of Palaeogene sandstones in the Padesh strike-slip basin. *Southwestern Bulgaria Geologica Balcanica* 43(1–3):3–26
- Corbett PWM, Potter DK (2004) Petrotyping: A base map and Atlas for navigating through permeability and porosity data for reservoir comparison and permeability prediction. In: International symposium of the Society of core analysts. SCA2004–30:1–12
- EGPC (1994) Nile Delta and north Sinai Fields, discoveries and hydrocarbon potential (a comprehensive overview). The Egyptian Petroleum Corporation, Cairo, p 387p
- El-Heiny I, (1982) Neogene stratigraphy of Egypt. *News 1. Stratigraphy II*:41–54
- El Heiny I, Enani N (1996) Regional stratigraphic interpretation pattern of Neogene sediments, northern Nile Delta, Egypt, 13th EGPC Expl. Prod. Conf. Cairo, Egypt 1:270–290
- El Sharawy MS, Nabawy BS (2018) Determining the porosity exponent  $m$  and lithology factor  $a$  for sandstones and their control by overburden pressure: a case study from the Gulf of Suez. *Egypt AAPG Bulletin* 102(9):1893–1910
- El Heiny I, Rizk R, Hassan M (1990) Sedimentological model for Abu Madi reservoir sands, Abu Madi field, Nile Delta, Egypt. 10th EGPC Expl. Prod. Conf. Cairo, Egypt 2:515–551
- El Sawy MZ, Abuhagaza AA, Nabawy BS, Lashin A (2020) Rock typing and hydraulic flow units as a successful tool for reservoir characterization of Bentiu-Abu Gabra sequence, Muglad basin, southwest Sudan. *J Afr Earth Sci* 171:103961
- Elgendy NTH, Abuamarah BA, Nabawy BS, Ghrefat H, Kassem OMK (2020) Pore fabric anisotropy of the cambrian-ordovician nubia sandstone in the onshore Gulf of Suez, Egypt: a surface outcrop analog. *Nat Resour Res* 29(2):1307–1328
- El-Ghali MAK, El Khoriby E, Mansurbeg H, Morad S, Ogle N (2013) Distribution of carbonate cements within depositional facies and sequence stratigraphic framework of shoreface and deltaic arenites, Lower Miocene, the Gulf of Suez rift. *Egypt J Marine Petrol Geol* 45:267–280
- Elhamy AT, Salah SA (2016) Structural effect on hydrocarbon trapping, North Western Nile Delta, Egypt. *Inter Jour Geosci* 7:353–366
- El-HeinyMorsi IS (1992) Stratigraphic correlation of Neogene sediments in the eastern Nile Delta and Gulf of Suez. 11th EGPC Expl. Prod. Conf. Cairo, Egypt 1:166–193
- Elhossainy MM, Abdelmaksoud A, Ali M, Alrefae HA (2021) Integrated sedimentological and petrophysical characterization of the lower Cenomanian clastic Bahariya reservoir in Abu Gharadig Basin, Western Desert. *Egypt J Afr Earth Sci* 184:104380
- Elmahdy M, Radwan AA, Nabawy BS, Abdelmaksoud A, Nastavkin AV (2023) Integrated geophysical, petrophysical and petrographical characterization of the carbonate and clastic reservoirs of the Waihapa Field, Taranaki Basin, New Zealand. *Mar Pet Geol* 15:106173
- Fallah-Bagtash R, Adabi MH, Nabawy BS, Omidpour A, Sadeghi A (2022) Integrated petrophysical and microfacies analyses for a reservoir quality assessment of the Asmari Dolostone sequence in the Khesht Field, SW Iran. *J Asian Earth Sci* 223:104989
- Fawzy A, El Rawy A, Lala A (2022) Estimation of net-pay thickness, using seismic reflectivity and band-limited impedance approaches, Central Nile Delta, Egypt. *J Appl Geophys* 21(2):99–112
- Fea I, Abioui M, Nabawy BS, Jain S, Bruno DZ, Kassem AA, Bensaou M (2022) Reservoir quality discrimination of the Albian-Cenomanian reservoir sequences in the Ivorian basin: a lithological and petrophysical study. *Geomech Geophys Geo-Energy Geo-Resour* 8(1):1
- Ghoneimi A, Ibrahim ShA, El-Kenawy A, Farrag Kh (2017) Use of well-logs for petrophysical evaluation of Abu Madi Reservoir In Abu Madi - El-Qara - Nidoco Area, Northern Nile Delta. *Egypt Bullet Facult Sci Zagazig Univ* 39:280–304
- Harms JC, Wray JL (1990) Nile Delta. In: Said R (Ed.), *the geology of Egypt*, A.A. Balkema, Rotterdam, Brookfield, 329–343.
- James NP (1978) Neritic carbonate depositional environments. In: *Sedimentology. Encyclopedia of Earth Science*. Springer, Berlin, Heidelberg. [https://doi.org/10.1007/3-540-31079-7\\_145](https://doi.org/10.1007/3-540-31079-7_145)
- Kamel H, Eita T, Sarhan M (1998) Nile Delta hydrocarbon potentiality, 14th EGPC Expl. Prod. Conf. Cairo, Egypt 1:485–503
- Kassem AA, Osman OA, Nabawy BS, Baghdady AR, Shehata AA (2022) Microfacies analysis and reservoir discrimination of channelized carbonate platform systems: an example from the Turonian Wata Formation, Gulf of Suez, Egypt. *J Petrol Sci Eng* 212:110272
- Khaled KA, Attia GM, Metwalli FI, Fagelnour MS (2014) Subsurface geology and petroleum system in the Eastern Offshore Area, Nile Delta, Egypt. *J Appl Sci Res* 10(4):254–270
- Khater GA, Nabawy BS, Kang J, Yue Y, Mahmoud MA (2020) Magnetic and electrical properties of glass and glass-ceramics based on Weathered Basalt. *SILICON* 12(12):2921–2940
- Kirschbaum MA, Schenk CJ, Charpentier RR, Klett TR, Brownfield ME, Pitman JK, Cook TA, Tennyson ME (2010) Assessment of undiscovered oil and gas resources of the Nile Delta Basin Province, Eastern Mediterranean. *USGS Bulletin, Fact Sheet*, 1–4.
- Leila M, Kora MA, Ahmed MA, Ghanem A (2016) Sedimentology and reservoir characterization of the Upper Miocene Qawasim Formation, El-Tamad Oil Field onshore Nile Delta Egypt. *Arab J Geosci* 9(1):1–13
- Leila M, Eslam A, El-Magd AA, Alwaan L, Elgendy A (2021) Formation evaluation and reservoir characteristics of the Messinian Abu Madi sandstones in Faraskour Gas Field, onshore Nile Delta. *Egypt J Petrol Explor Product Technol* 11:133–155
- Leila M, El-Sheikh I, Abdelmaksoud A, Radwan AA (2022) Seismic sequence stratigraphy and depositional evolution of the Cretaceous-Paleogene sedimentary successions in the offshore Taranaki Basin, New Zealand: implications for hydrocarbon exploration. *Marine Geophys Res* 43(2):23. <https://doi.org/10.1007/s11001-022-09483-z>
- Longman MW (1980) Carbonate diagenetic textures from near-surface diagenetic environments. *Bullet Am Assoc Petrol Geol* 64:461–487
- Lukasik JJ, James NP, McGowran B, Bone Y (2000) An epeiric ramp: low-energy, cool-water carbonate facies in a Tertiary inland sea, Murray Basin, South Australia. *Sedimentology* 47(4):851–881
- Mahsoub MA (2006) Facies and stratigraphy of the sedimentary sequence of Abu Qir West Field, Nile Delta-Egypt, unpublished M. Sc. thesis, Ain Shams Univ., Egypt, 220 p.
- Mosconi A, Rebora A, Venturino G, Bocca P, Khalil H (1996) Egypt -Nile Delta and North Sinai Cenozoic tectonic evolutionary model - A proposal, EGPC., Proc. of the 13th EGPC Expl. Prod. Conf., Cairo, Egypt, 1:203-223
- Nabawy BS (2018) Impacts of fossil anisotropy on the electric and permeability anisotropy of highly fossiliferous limestone: a case study. *Mar Geophys Res* 39(4):537–550



- Nabawy BS, El Aal AA (2019a) Impacts of the petrophysical and diagenetic aspects on the geomechanical properties of the dolomitic sequence of Gebel El-Halal, Sinai. *Egypt Bull Eng Geol Environ* 78(4):2627–2640
- Nabawy BS, El Aal AA (2019b) Effects of diagenesis on the geomechanical and petrophysical aspects of the Jurassic Bir El-Maghara and Masajid carbonates in Gebel El-Maghara, North Sinai. *Egypt Bull Eng Geol Environ* 78(7):5409–5429
- Nabawy BS, El Sharawy MS (2018) Reservoir assessment and quality discrimination of Kareem Formation using integrated petrophysical data, Southern Gulf of Suez. *Egypt Mar Petrol Geol* 93:230–246
- Nabawy BS, Shehata AM (2015) Integrated petrophysical and geological characterization for the Sidi Salem-Wakar sandstones, off-shore Nile Delta. *Egypt J Afr Earth Sci* 110:160–175
- Nabawy BS, Wassif NA (2017) Effect of the mineralogical composition on the petrophysical behavior of the amygdaloidal and vesicular basalt of Wadi Wizr, Eastern Desert. *Egypt J Afr Earth Sci* 134:613–625
- Nabawy BS, Rochette P, Géraud Y (2010) Electric pore fabric of the Nubia sandstones in south Egypt: characterization and modeling. *Geophys J Int* 183(2):681–694
- Nabawy BS, Sediek KN, Nafee SA (2015) Pore fabric assignment using electrical conductivity of some Albian-Cenomanian sequences in northeastern Desert, Egypt. *Egypt Arab J Geosci* 8(8):5601–5615
- Nabawy BS, Basal AMK, Sarhan MA, Safa MG (2018) Reservoir zonation, rock typing and compartmentalization of the Tortonian-Serravallian sequence, Temsah gas field, offshore Nile delta. *Egypt Mar Petrol Geol* 92:609–631
- Nabawy BS, Ibrahim E, Kahal A, Alfaifi HJ, Lashin AA (2020a) Impact of authigenic iron oxides, clay content, and grain size on the aquifer quality properties of the Cambrian-Ordovician Wajid Sandstone, southwest Saudi Arabia. *J Afr Earth Sci* 172:104000
- Nabawy BS, Khalil HM, Fathy MS, Ali F (2020b) Impacts of microfacies type on reservoir quality and pore fabric anisotropy of the Nubia sandstone in the central Eastern Desert, Egypt. *Geol J* 55(6):4507–4524
- Nabawy BS, Mansour AS, Rashed MA, Afify WSM (2020c) Implementation of sedimentary facies and diagenesis on the reservoir quality of the Aquitanian-Burdigalian Rudeis Formation in the Gulf of Suez, Egypt: a comparative surface and subsurface study. *Geol J* 55(6):4543–4563
- Nabawy BS, Abudeif AM, Masoud MM, Radwan AE (2022a) An integrated workflow for petrophysical characterization, microfacies analysis, and diagenetic attributes of the Lower Jurassic type section in northeastern Africa margin: implications for subsurface gas prospecting. *Mar Pet Geol* 140:105678
- Nabawy BS, Lashin AA, Barakat MKh (2022b) Implementation of lithofacies and microfacies types on reservoir quality and heterogeneity of the Late Cretaceous Upper Bahariya Member in the Shouk Field, Shoushan Basin, North Western Desert, Egypt. *J Asian Earth Sci* 224:105014
- Nabawy BS, Abd El Aziz EA, Ramadan M, Shehata AA (2023) Implication of the micro- and lithofacies types on the quality of a gas-bearing deltaic reservoir in the Nile Delta. *Egypt Sci Rep* 13(1):8873
- Niazi M, Dahi M (2004) Un-Explored Giant Sandstone Features in Ultra-deep water, West Mediterranean, Egypt. *AAPG International Conference* 24–27.
- Othman A, Fathy M, Matresu J, Nassar M (2022) Integration of 3D seismic attributes and production history in reevaluation of gas potential - Abu Madi and El Qaraa fields. *Delta J Sci* 44(1):123–134
- Pigott JD, Abdel-Fattah MI (2014) Seismic stratigraphy of the Messinian Nile delta coastal plain: recognition of the fluvial regressive systems tract and its potential for hydrocarbon exploration. *J Afr Earth Sci* 95:9–21
- Radwan AA, Nabawy BS (2022) Hydrocarbon prospectivity of the miocene-pliocene clastic reservoirs, Northern Taranaki Basin, New Zealand: Integration of Petrographic and Geophysical Studies. *J Petrol Explor Product Technol* 12(7):1945–1962
- Radwan AA, Nabawy BS, Abdelmaksoud A, Lashin A (2021) Integrated sedimentological and petrophysical characterization for clastic reservoirs: a case study from New Zealand. *J Natl Gas Sci Eng* 88:103797
- Radwan AA, Abdelwahhab MA, Nabawy BS, Mahfouz KH, Ahmed MS (2022a) Facies analysis-constrained geophysical 3D-static reservoir modeling of Cenomanian units in the Aghar Oilfield (Western Desert, Egypt): Insights into paleoenvironment and petroleum geology of fluviomarine systems. *Mar Pet Geol* 136:105436
- Radwan AA, Nabawy BS, Shihata M, Leila M (2022b) Seismic interpretation, reservoir characterization, gas origin, and entrapment of the Miocene-Pliocene Mangaa C sandstone, Karewa Gas Field, North Taranaki Basin, New Zealand. *Mar Petrol Geol* 135:105420
- Rizzini A, Vezzani F, Coccecca V, Milad G (1978) Stratigraphy and sedimentation of Neogene-Quaternary section in the Nile Delta area. *Marine Geol* 27:327–348
- Safa MG, Nabawy BS, Basal AMK, Omran MA, Lashin A (2021) Implementation of a petrographical and petrophysical workflow protocol for studying the impact of heterogeneity on the rock typing and reservoir quality of Reefal limestone: a case study on the nullipore carbonates in the Gulf of Suez. *Acta Geol Sin* 95(5):1746–1762
- Said R (1981) *The geological evolution of the River Nile*. Springer, Verlag, p 151
- Salem AM, Ketzer JM, Morad S, Rizk RR, Al-Aasm IS (2005) Diagenesis and reservoir-quality evolution of incised valley sandstones: evidence from the Abu Madi gas reservoirs (Upper Miocene), the Nile Delta Basin, Egypt. *J Sed Res* 75:572–584
- Sarhan MA (2021a) Assessing hydrocarbon prospects in Abu Madi Formation using well logging data in El-Qara field, Nile Delta Basin. *Egypt J Petrol Explor Prod Technol* 11(6):2539–2559
- Sarhan MA (2021b) Gas-generative potential for the post-Messinian mega-sequence of Nile Delta Basin: a case study of Tao field, north Sinai concession. *Egypt J Petrol Explore Prod* 12:925–947. <https://doi.org/10.1007/s13202-021-01354-4>
- Sarhan MA (2022) Geophysical appraisal of the Abu Madi gas reservoir, Nile Delta Basin, Egypt: implications for the tectonic effect on the lateral distribution of petrophysical parameters. *Petrol Res* 7(4):511–520
- Sarhan MA, Safa MG (2019) 2D seismic interpretation and hydrocarbon prospects for the Neogene-Quaternary succession in the Temsah Field, offshore Nile Delta Basin. *Egypt J Afr Earth Sci* 155:1–12
- Sarhan M, Hemdan K (1994) North Nile delta structural setting trapping and mechanism, in Egypt. *Proc. 12th EGPC Expl. Prod. Conf.*, Cairo, Egypt 1:1–18
- Schlumberger (1984) Well evaluation conference, Egypt. *Geology of Egypt*, 1–64 p.
- Serra O (1988) *Fundamentals of well-log interpretation*. 1. The acquisition of logging data. 3rd Ed., Elsevier, Amsterdam, 423p.
- Sestini G (1989) Nile Delta: A review of depositional environments and geological history. In: Whateley MKG, Pickering KT (eds), *Deltas: sites and traps for fossil fuels*. Geological Society London, Special Publication 41:99–127.
- Shehata AA, Osman OA, Nabawy BS (2021) Neural network application to petrophysical and lithofacies analysis based on multi-scale data: an integrated study using conventional well log, core, and borehole image data. *J Natl Gas Sci Eng* 93:104015
- Shenawi SH, White JP, Elrafie EA, Kilany KA (2007) Permeability and water saturation distribution by lithologic facies and hydraulic

- units: A Reservoir Simulation Case Study: Society of Petroleum Engineers Paper no. 105273. In 15th Society of Petroleum Engineers Middle East Oil & Gas Show and Conference, Kingdom of Bahrain.
- Sultan MO, El-Barhooky AN, El-Araby AM (2020) Reservoir characterization of the upper miocene, using seismic and well log data in the Northeastern Onshore Area of the Nile Delta, Egypt. *Egypt J Appl Geophys* 19(2):1–10
- Teama MA, Nabawy BS (2016) Petrophysical evaluation of the hydrocarbon potential of the Lower Cretaceous Kharita clastics, North Qarun oil field, Western Desert. *Egypt J Afr Earth Sci* 121:62–71
- Teh WJ, Willhite GP, Doveton JH (2012) Improved reservoir characterization using petrophysical classifiers within electrofacies. Society of Petroleum Engineers, SPE-154341-PP.
- Vandre C, Cramer B, Gerling P, Winsemann J (2007) Natural gas formation in the western Nile delta (Eastern Mediterranean): thermogenic versus microbial. *Org Geochem* 38:523–539
- Winland HD (1972) Oil accumulation in response to pore size changes, Weyburn field, Saskatchewan. Amaco Production Research Report No. F72-G-25.

**Publisher's Note** Springer Nature remains neutral with regard to jurisdictional claims in published maps and institutional affiliations.